Estimating Parameters for a Doyle Fuller Newman Model of a Graphite Half Cell Battery

A Dissertation
Presented to
The Academic Faculty

by

Gregory Dan Chipman

In Partial Fulfillment
of the Requirements for the Degree
Master of Science in the
School of Chemical & Biomolecular Engineering

Georgia Institute of Technology
August 2020

Estimating Parameters for a Doyle Fuller

Newman Model of a Graphite Half Cell Battery

Approved by:

Dr. Tom Fuller, Advisor
School of Chemical Engineering
Georgia Institute of Technology

Dr. Paul Kohl
School of Chemical Engineering
Georgia Institute of Technology

Dr. Elsa Reichmanis
School of Chemical Engineering
Georgia Institute of Technology

Date Approved: [Month dd, yyyy]

ACKNOWLEDGEMENTS

There are many people to who I am grateful for helping me during my time at Georgia Tech. The road has been a long and difficult one for me. One that I could not have endured without the help of friends, family, work associates, and professional help. I would first like to thank my graduate advisor, Dr. Tom Fuller, for his guidance and help and for his patience with me. I would also like to thank many of the class mates I have had while being here, including many from my cohort and also those who I have had the pleasure of working with in the Fuller lab. Primarily, I would like to thank my roommate of 4 years, Thomas Kwok, who helped me to get through the classes early on and was always encouraging me even as I struggled through research. While here, I have had the opportunity to work on improving my mental health and I would like to thank everyone at Georgia Tech and my counselor at Atlanta Center for Cognitive Therapy for helping me to learn and grow during my time here. Lastly, I would like to thank my parents and siblings and extended family for always supporting me and believing in me every step of the way. I have a hard time believing in myself so having the support of each and every one of you has helped me to push through and succeed. Thank you to everyone that believed in me in spite of the many setbacks and struggles that I had. It has made all the difference.

TABLE OF CONTENTS

LIST OF TABLES

LIST OF FIGURES

LIST OF SYMBOLS AND ABBREVIATIONS

BMS	Battery Management Systems
cf	Correction Factor
CPE	Constant Phase Element
CV	Cyclic Voltammetry
DFN	Doyle Fuller Newman
ECM	Equivalent Circuit Model
EIS	Electrochemical Impedance Spectroscopy
GITT	Galvanostatic Intermittent Titration Technique
SEI	Solid Electrolyte Interphase
SEM	Scanning Electron Microscope
SOC	State of Charge
A	Superficial Surface Area
a	Specific Interfacial Area
c_{el}	Electrolyte Lithium-ion Concentration
c_s	Graphite Solid Phase Lithium Concentration
$c_{s,max}$	Maximum Graphite Solid Phase Lithium Concentration
D	Average Value of the Solid Phase Diffusivity Coefficients
D_{el}	Lithium-ion Diffusivity in Electrolyte
$D_{el_{eff}}$	Lithium-ion Effective Diffusivity in Electrolyte
D_s	Lithium Diffusivity in Graphite Solid Phase Particles
F	Faraday's Constant
i	Square Root of -1

i_1	Graphite Solid Phase Current
i_2	Electrolyte Current
j	Interfacial Current
j_0	Exchange Current Density
L	Separator Thickness
N	Constant Phase Element Exponent
N_{Li^+}	Molar Lithium-ion Flux
Ne	Newman Number
R	Universal Gas Constant
r	Radius
R_{ct}	Charge Transfer Resistance
R_{ohmic}	Ohmic Resistance
T	Temperature
t	Time
t^+	Transference Number
U	Equilibrium Potential
V	Volume
V_M	Molar Volume
X	Thickness
Y	Admittance
z	Ion Charge
Z_{CPE}	Constant Phase Element Impedance
Z_W	Warburg Impedance
α	Charge Transfer Coefficient

α_a	Anodic Charge Transfer Coefficient
α_c	Cathodic Charge Transfer Coefficient
δ	Nernst Diffusion Layer Thickness
ε	Porosity
κ	Electrolyte Conductivity
κ_{eff}	Electrolyte Effective Conductivity
η	Overpotential
ϕ_1	Graphite Solid Phase Potential
ϕ_2	Electrolyte Potential
σ	Warburg Coefficient from PyCharm Fitting
σ_W	Warburg Coefficient from Slope of Impedance vs the Inverse Square Root of Frequency
σ_{eff}	Graphite Solid Phase Effective Conductivity
τ	Tortuosity
ω	Frequency

SUMMARY

Electrochemical research involves the modeling of electrochemical systems using various types of models. Models use adjustable parameters to be able to fit experimental data. Parameters of physics-based models are actual properties of the electrochemical system; and, if determined accurately, can reveal more about the inner physics of the system. Further physics-based models can be extrapolated with more confidence to other experimental conditions. Because insights obtained and ability to extrapolate from a physics-based model is based on the accuracy of the parameters obtained, the main objective of adjusting the parameters to fit the experimental data should be finding the most accurate parameter set, not the best fitting parameter set. Because of the complexity of physics-based models, adjusting parameters to fit experimental data without forethought and estimates may lead to inaccurate parameter sets.

This thesis focused on laying out a procedure for estimating parameters for a physics-based model to increase the probability of obtaining an accurate parameter set for the electrochemical system. As an example, parameters were obtained for a Doyle Fuller Newman model for a graphite vs. lithium coin cell battery. These estimates were obtained from scanning electron microscopy images, the galvanostatic intermittent titration technique, and electrochemical impedance spectroscopy. These estimates were put into a Doyle Fuller Newman model in gPROMs and the simulation output was compared to experimental discharge data. These estimates can be used as a starting point for fitting the model to experimental data to find a final set of parameters for the model.

CHAPTER 1. INTRODUCTION

Batteries have become increasingly widespread as a power source for many of the world's modern technologies. Laptops and cell phones have become a staple of a majority of United States adults' lifestyles. A study stated that as of 2019 96% of U.S. adults own a cell phone, with 81% owning a smart phone.[1] Cell phones are typically powered by lithium-ion batteries that companies continually research to improve energy and power density, safety, economic viability, lifespan, and charging time. Lithium-ion batteries have also emerged as the primary power source for electric vehicles in the automotive sector. The need for improvement here is perhaps greater than with consumer devices as the viability of electric vehicles depends on meeting consumers' desired specifications, which are influenced by their experience with the internal combustion engine. Some common ones include increasing the driving range on one charge, decreasing charging time, and increasing the power density of the battery pack. One major push for the electrification of the automotive industry is to decrease greenhouse emissions.[2] However, the use of electric vehicles is only as environmentally responsible as the energy source used to produce the electricity at the power plant.[3] Batteries can also play an important role here as they can store the energy produced by renewable resources like solar and wind that tend to be more intermittent than those produced by coal, nuclear, and natural gas power plants.[4] The storage of power produced by renewable energy sources would allow a power plant to store excess energy during times of low demand to be used at times when demand increases. Batteries and other electrochemical energy storage devices will play a central role in many of the current and future technologies that we use as well as the push to decrease our

environmental footprint. However, many improvements are both necessary and desired for that future to be realized.

To improve batteries, research is conducted at universities, corporations, and national labs to try to find new materials (electrodes, electrolytes, separators), improve current materials, and to better understand the physics behind battery function.[5-7] One way to improve understanding of the electrochemical processes that occur in batteries is the use of physics-based models. Physics-based models attempt to accurately depict what is happening in the electrochemical system using material and energy balances and phenomenological equations such as Ohm's law and the Butler-Volmer equation. This approach contrasts with equivalent circuit models (ECMs) that represent the same behaviors by using circuit elements, resistors, capacitors, and voltage sources, to approximate the physical behavior taking place. As an introduction to ECMs, each of the circuit elements commonly used to represent an electrochemical system will be detailed below. The following summary is based largely on Plett's book chapter on ECMs.[8]

An ECM starts by representing the electrochemical system as a voltage source. The voltage is constant and, at this point, isn't a very good model of an actual electrochemical system. Other circuit elements are added to the ECM to improve the accuracy of the model, until the model is found to be a sufficient approximation of the electrochemical system for the purpose of the modeler. Some common additions include modeling the dependence of the equilibrium voltage on state of charge (SOC). This is because the equilibrium voltage commonly changes with SOC, or how many coulombs have passed through the electrochemical system. This SOC dependent equilibrium voltage is then used as a starting place for other circuit elements to be added.

These other circuit elements are added to represent the polarizations experienced by the electrochemical system. Polarizations are reasons why the voltage of the electrochemical system differs from the equilibrium voltage when the electrochemical system is not at equilibrium. Three polarizations that are most often seen in electrochemical systems are an ohmic polarization, a kinetic polarization, and a concentration polarization. The ohmic polarization is caused by the voltage loss induced by current flowing through the electrochemical system. The amount of the ohmic voltage loss is primarily related to the conductivity of the materials of the electrochemical system. To represent the ohmic polarization in an ECM, a resistor can be added that is termed the equivalent series resistance. This is a resistor that changes the voltage based on the current applied to the electrochemical system by multiplying the current by the equivalent series resistance representing the ohmic polarization. To represent the charge transfer polarization, a resistor in parallel with a capacitor is added. The capacitor represents the double layer capacitance, the accumulation of charge on the surface of the electrode. The resistor represents the charge transfer resistance, the voltage change associated with the electrochemical reaction. Lastly, a Warburg impedance, which is an infinite series of resistors and capacitors in parallel, is added to represent the concentration polarization. A concentration polarization is caused by the resistance to mass transport of the electrochemical system causing concentration gradients. The mass transport polarization refers to how these concentration gradients change the voltage of the electrochemical system. Most ECMs use a combination of these circuit elements to model the behavior of the electrochemical system being simulated.

Once an ECM has been applied to an electrochemical system, the parameters, resistances, capacitances, etc., used for each of the circuit elements are extracted by fitting experimental data. Extracting parameters from experimental data means adjusting circuit parameters to obtain the best fit possible to an experimental data set. This is often done using computers to minimize the difference between the simulations and the experimental data set. Estimates can be obtained for individual ECM parameters from specific sets of experimental data. These estimates can then be used for the overall fitting of the ECM to all of the experimental data being used. Using parameter estimates can improve the final parameter set obtained. For example, the equivalent series resistance can be estimated from the instantaneous change in voltage after a step change in current. This estimate for the equivalent series resistance can be used along with other parameter estimates as a starting place for extracting each of the necessary parameters. Once the final parameter set has been selected by fitting the ECM to experimental data, it is often then compared to a validation data set. A validation data set is a set of experimental data that was not used in the original extraction. Comparing the ECM output to the validation data set helps to ensure that the ECM can match experimental data beyond that which was used in the parameter extraction process without needing to further adjust parameters. Once an ECM is fully parameterized it can be used to predict the current and voltage relationship for the electrochemical system.

Battery management systems (BMS) use models to estimate conditions of the battery that are needed to maintain the safety and health of the battery. BMS provide an example to help explain the reasons for using ECMs or physics-based models to model an electrochemical system. ECMs are often used in battery management systems (BMS) because they provide the necessary information and are less complex than physics-based

models. When ECMs are used in BMS for portable electronics they are able to perform adequately. However, Chaturvedi et al. showed ECMs struggle in BMS for automotive applications due to differences in cycling rates and the need to continue to add additional circuit elements to be able to adequately represent the electrochemical system.[9] Additionally, ECMs only provide information on the current and voltage of the electrochemical system. Physics-based models are needed to gain additional insight into the electrochemical system such as concentration, voltage, and current profiles throughout the electrochemical system. Physics-based models can also be extrapolated to other experimental conditions whereas ECMs cannot be with the same level of confidence. ECMs are good for modeling the current-voltage relationship of electrochemical systems while minimizing the complexity of the model. Physics-based models are good for gaining additional understanding of the electrochemical system. In research, physics-based models are often preferred because of the additional insight they provide.

While physics-based models provide additional understanding, they can be more difficult to fit to experimental data than ECMs. The benefit of an ECM model is the ability to fit experimental data well with a simpler model. However, the parameters of an ECM are not directly related to physical parameters of the electrochemical system. Physics-based model's parameters, on the other hand, are, and because they are physical parameters of the electrochemical system, they are well-defined and have true immutable values. When parameterizing a physics-based model the goal is to obtain values as close to these true-immutable values as possible. The only visible way to assess the accuracy of the parameters is to compare the output of the model to experimental data. When a physics-based model compares well to experimental data it increases the modeler's confidence that the true

values for the parameters have been obtained. Which provides additional confidence in using the model outside of the range of the experimental data and the additional insights provided by the physics-based model. The value in a physics-based model lies in the confidence the modeler has that they have found the actual values for each of the parameters of the electrochemical system. The information gathered from a physics-based model, as far as increasing physical understanding of the system being investigated, is only as accurate as the physical parameters identified for the materials being used.[10]

However, even when using physics-based models, there is still a temptation to prioritize fitting the experimental data rather than obtaining an accurate parameter set for the electrochemical system. While fitting experimental data is the main way to assess the accuracy of a model, there are cases where a model can fit experimental data sets using parameters that are infeasible or incorrect. Since fitting the experimental data provided does not guarantee that the parameter set identified is accurate, fitting the experimental data cannot be the only focus of determining parameters in a physics-based model. To increase the probability of finding the true values for each of the physical parameters of the electrochemical system, a process must be established that helps the modeler to follow a methodology that reduces the chance of finding infeasible or inaccurate physical parameters.

Finding an accurate set of parameters is one of the main challenges of model parameterization. While some parameters can be determined by direct measurement, like the thickness of the electrode or the separator, most parameters are currently determined by fitting model results to experimental data.[11] Parameters are usually determined either by using the personal experience and knowledge of a battery modeler, or, more recently,

the use of data science.[12] These methods can be effective, but both can give parameters that are physically unreasonable. At times, a large number of parameters have been extracted simultaneously by fitting experimental data.[13] The accuracy of the parameter set determined by fitting experimental data is difficult to assess because fitting experimental data by adjusting parameters is complex on several levels. Common physics-based battery models have on the order of 50 parameters that all interact and are difficult to isolate to determine them independently. In theory, a certain experimental data set may be fit equally well by two or more different parameter sets due to the interaction of these parameters. The process for parameter identification for physics-based models needs to be more well-defined, and include more than just fitting experimental data, to increase the confidence of the modeler in the accuracy of the parameters obtained.

One common pitfall of parameter identification is the focus on a select set of experimental data.[14] While the parameters may fit the original set of experimental data well, using the same parameters for a different set of experimental data (e.g., Cyclic Voltammetry (CV) vs. cycling) can lead to results that do not come close to matching the new set of experimental data. The concern of a set of parameters not fitting other data sets is often mitigated by using a training set and a validation set to ensure that the parameter set fits data other than the data used for fitting.[15] However, depending on the data used for validation, there still remain concerns about extending a model beyond its limitations. For example, if a parameter set for a model is determined by using discharge data and validated using charging data, there would be no guarantee that the data would match other testing conditions like cyclic voltammetry or high pulse power current test. Tests that are common in electric vehicle characterization that use higher and more varied currents than normal

cycling data.[16-17] Since one of the primary purposes of the physics-based model is to highlight areas where understanding is lacking, it is important that the model be valid for a variety of experimental data.[18] This highlights another area that should be covered in a process for identifying parameters for a physics-based model.

Because of the desire to improve electrochemical systems, there have been many papers written on physics-based models and their parameterization. Before refining parameters by fitting experimental data, an estimate, or initial starting point, must be identified to put into the model.[19] The obtaining of these physical parameter estimates is one area that is often glossed over or neglected in papers detailing physics-based model parameterization. If they do mention how estimates for the parameters were obtained, it is usually from a literature search to find parameter estimates for similar electrochemical systems.[20] However, the literature values can vary by several orders of magnitude for certain parameters making it difficult to find a reasonable estimate. For example, Less et al. pointed out that the experimental values of the solid phase diffusivity of a Li-ion in lithium-manganese oxide spans four orders of magnitude (10^{-9}-10^{-12} cm^2s^{-1}) in the literature.[19] Even if values in a literature search were viable for well-established materials, it is not possible for new materials. One solution to improve confidence in parameter estimates obtained for well-established materials and to be able to obtain parameter estimates for new materials is to determine parameter estimates independently for the electrochemical system being modeled.

While many papers have identified parameters for models by fitting experimental data, there are not many papers that sufficiently outline the process for estimating parameters. Though there has been good work done by Ecker et al., Schmalstieg et al., and

Plett et al.[18,20-23] Obtaining a good estimate for physical parameters before fitting experimental data is important because different estimates can lead to very different results. Both because of the interaction of the parameters, and because of local minima that may cause the fitting process to finish prematurely. Identifying a reasonable estimate for each parameter would help improve the odds that the fitting process converges on the most accurate values for the system. A process for estimating parameters would be helpful as a starting point for later refining these parameters by fitting experimental data.[21] Reasonable estimates for physical parameters can improve the confidence in the accuracy of the parameters obtained from fitting, reduce the computational cost by improving the proximity of the estimates to the final values, and help to identify bounds for parameters that can be used for constrained optimization.

This thesis outlines a process for parameterizing a lithium-ion battery model shown in Figure 1. The process starts by identifying all the necessary model parameters. In this thesis, a Doyle Fuller Newman (DFN) model was constructed to simulate a graphite vs. lithium coin cell. The needed physical parameters for the model will be outlined in Chapter 2. The process then outlines how to find estimates for each of the physical parameters either through measuring, calculating, or experiments. Measuring the parameter values, as mentioned previously, is ideal and as many parameters as possible should be measured. However, it is up to the modeler to determine what parameters they have the experimental capability and knowledge to measure directly. In this thesis, the particle radius and electrode thickness were measured using SEM imaging. This is shown in Chapter 3. While other parameters could be measured like the porosity or the conductivity they were not measured in this thesis. Instead, the porosity was taken from the literature and the

conductivity was estimated from EIS data which was then compared to the literature. This was a decision made due to the modeler not having the experimental capability and knowledge set to measure these parameters directly. The experiments used as part of the process for estimating the physics-based model's parameters include the galvanostatic intermittent titration technique (GITT), outlined in Chapter 3, and electrochemical impedance spectroscopy (EIS), outlined in Chapter 4. The EIS data is fit to an ECM and the ECM parameters are used to estimate physical parameters. While ECM parameters are not directly related to physical parameters, work has been done previously to use ECM parameters fit to EIS data to estimate physical parameters. Once estimates have been obtained for all the parameters needed for the model, model results using the parameter estimates are compared to experimental discharge data in Chapter 5.

The focus of this thesis was to outline a process to obtain estimates for the parameterization of a DFN model. However, future work should be conducted to detail a process for refining the parameter estimates to final values by strategically fitting experimental data. Future work can also be done on how to best validate the final parameter set using additional experimental data. By obtaining reasonable estimates, there will be an improved chance of maintaining final parameter sets that are logical, feasible, and accurate.

This thesis demonstrates the proposed parameter estimation process for a DFN model of a graphite vs. lithium coin cell. Experiments and equations are given to obtain the thermodynamic, kinetic, mass transport, and all other necessary parameters for the physics-based battery model. The model is then constructed in gPROMS, an equation-oriented modelling platform, and the results of the model using the parameter estimates obtained is compared to experimental discharge results.[24]

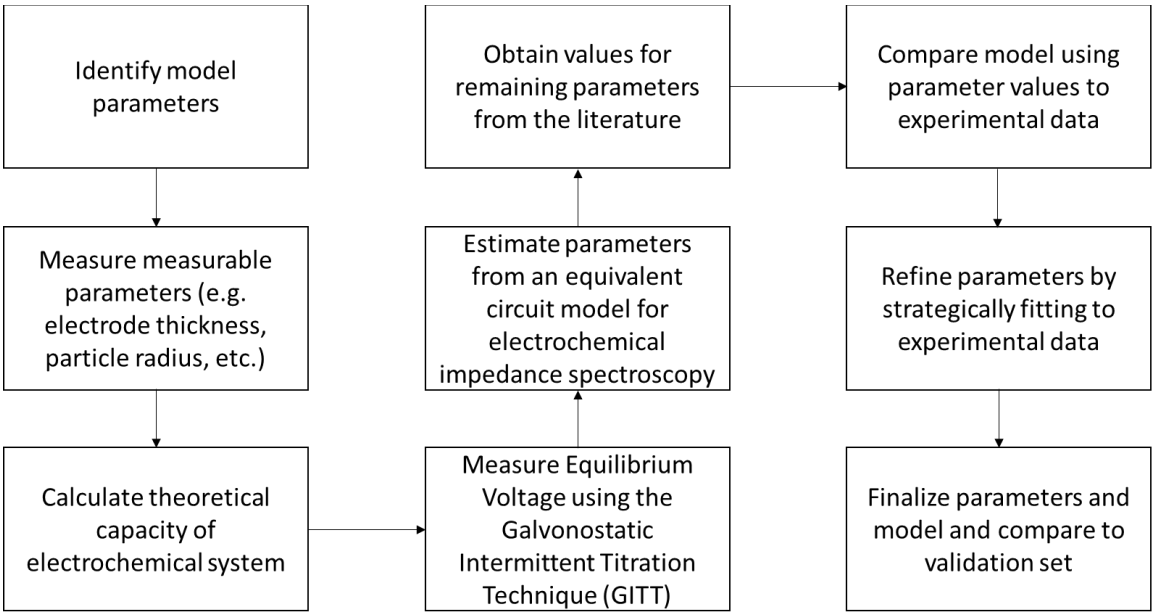

Figure 1 Proposed process for model parameterization

CHAPTER 2. PHYSICS BASED MODELING OF BATTERIES

There are a variety of models that are used to simulate battery performance. Two common types are physics-based models and equivalent circuit models (ECMs).[25] ECMs offer various benefits such as being simpler than physics-based models and being related to circuit elements that are widely available. However, ECMs are not always directly connected to physical parameters of the electrochemical system, do not provide additional information on the electrochemical system beyond the voltage and current, and cannot be extrapolated with much confidence to other experimental conditions. Because of the focus on wanting to better understand the physics of an electrochemical system, the model selected for this thesis was a physics-based model. Even when only considering physics-based models there are still many different types of models. Three common types include single particle models, lumped parameter models, and the Doyle Fuller Newman (DFN) model, a pseudo 2-D model.[26-28] While the principles of the parameter identification used in this thesis could be applied to any model, the DFN model was selected due to the prior knowledge base of the research group. Additionally, the DFN model is one of the most widely used physics-based models for batteries. The original paper having been cited thousands of times.[29]

The full details of the DFN model are explained in previous papers.[30-31] Included here is a summary to outline the necessary parameters for the DFN model. The first step in the proposed process for model parameterization in Figure 1. The DFN model is a pseudo 2-D model that primarily models the electrochemical system along the thickness of the cell. However, in the porous electrodes, the solid phase transport is modeled radially in the

particles of the electrode along the thickness of the electrode. In this thesis, a coin cell placing lithium foil vs. a graphite electrode was used. The materials used are specified in more detail in Chapter 3. Figure 2 shows a simplified representation of the lithium vs. graphite cell used in this thesis that helps to show the geometry used in the DFN model.

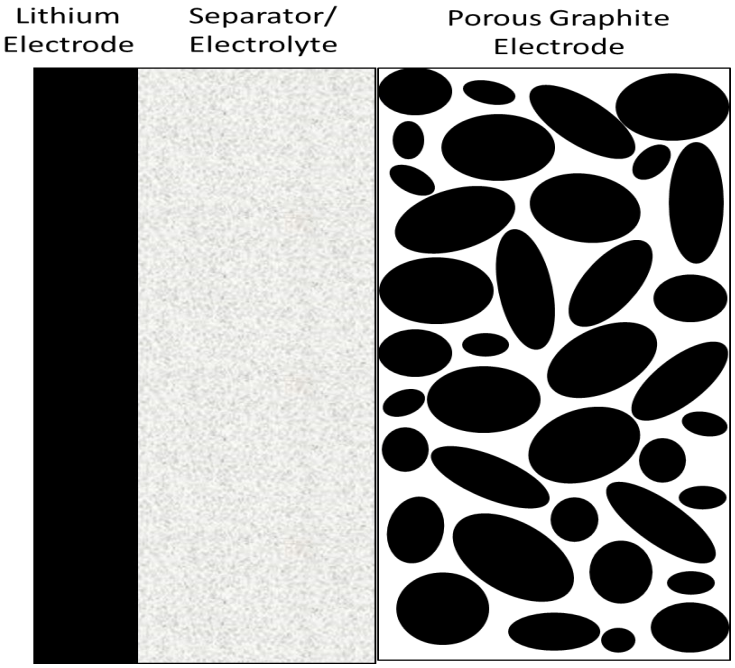

Figure 2 Representation of lithium vs graphite cell used in this thesis.

While the geometric parameters outline the area being modelled, the starting point for the voltage in the DFN model is the equilibrium voltage. All voltage losses caused by the kinetics, thermodynamics, and mass transport in the batteries modify the equilibrium voltage baseline to the actual voltage of the battery. This baseline is not constant as the equilibrium voltage changes as the battery is charged and discharged. The equilibrium voltage depends on the amount of lithium intercalated in the electrode, also known as the state of charge (SOC). SOC can be a bit ambiguous depending on how the modeler defines it. Sometimes, an SOC of zero does not refer to a fully unlithiated electrode, but rather to

a certain non-zero concentration. For example, it could be the solid phase concentration at the lower voltage cutoff for charging and discharging. Similarly, an SOC of one may not refer to a fully lithiated electrode depending on how the modeler defines it. A fully lithiated graphite electrode refers to the stoichiometry of the electrochemical equation for graphite. In this equation, lithium and graphite electrochemically interact to produce lithiated graphite, represented in the equation as LiC_6. When there is a mole of lithium for every six moles of graphite the electrode is considered fully lithiated. In this thesis an SOC of 0 refers to the completely unlithiated graphite electrode and an SOC of 1 refers to a fully lithiated graphite electrode. The equation for state of charge is shown below in Equation 1.

$$\mathrm{SOC} = \frac{c_s}{c_{s,max}} \tag{1}$$

Where c_s represents the solid phase lithium concentration in the graphite and $c_{s,max}$ represents the maximum lithium concentration for the graphite electrode.

The current in the electrode and electrolyte changes the voltage along the thickness of the electrode according to Ohm's law shown in Equations 2 and 3 for the electrode and electrolyte respectively. Equation 3 includes the modification for Ohm's law to account for concentration gradients.[32]

$$i_1 = -\sigma_{eff}\frac{d\phi_1}{dx} \tag{2}$$

$$i_2 = -\kappa_{eff}\frac{d\phi_2}{dx} + \frac{\kappa_{eff}\,R}{F}(1+TF)(1-t_{Li^+})\frac{d\,\ln(c_{el})}{dx} \tag{3}$$

Where i_1 and ϕ_1 represent the current and potential in the electrode (metal) and i_2 and ϕ_2 the same for the electrolyte. σ_{eff} and κ_{eff} represent the effective electrical conductivities for the electrode and electrolyte. R represents the universal gas constant, F represents Faraday's constant, and TF represents the thermodynamic factor, which is assumed to be 0 in this thesis. t_{Li^+}represents the transference number for lithium-ions in the electrolyte and c_{el} represents the lithium-ion concentration in the electrolyte. The equation for effective conductivity is shown in Equation 4.

$$\kappa_{eff_i} = \kappa \frac{\varepsilon_i}{\tau_i} \tag{4}$$

The electrolyte conductivity is multiplied by the porosity and divided by the tortuosity of the electrode, for the effective electrolyte conductivity in the electrode, or the porosity and tortuosity of the separator, for the effective electrolyte conductivity in the separator. The effective electrode conductivity is similarly found by multiplying by one minus the electrode porosity and dividing by the electrode tortuosity.

As mentioned above, the current through the electrode consists of two parts. The ionic current through the electrolyte and the electronic current through the electrode, i_2 and i_1 respectively. In the separator, the current is completely i_2 as there is only electrolyte. However, as the current enters the porous electrode part of the cell part of the current enters the electrode while part continues in the electrolyte. This change from ionic current to electronic current continues until the end of the electrode is reached, at which point the current is completely i_1. The flux, or change, from i_2 to i_1 is modeled using the Butler-Volmer expression shown in Equation 5.

$$j = j_0 \left[e^{\left(\frac{\alpha_a F \eta}{RT}\right)} - e^{\left(\frac{-\alpha_c F \eta}{RT}\right)} \right] \quad (5)$$

j_0 represents the exchange current density, which is the current density at the electrode electrolyte interface at equilibrium (when the cathodic and anodic reactions are occurring at the same rate). η is the overpotential, which is the difference between the electrode and electrolyte potential from the equilibrium voltage of the electrode. This is shown in Equation 6.

$$\eta = \phi_1 - \phi_2 - U \quad (6)$$

Where ϕ_1 represents the metal potential, ϕ_2 represents the potential of the electrolyte, and U represents the equilibrium potential of the electrode. ϕ_1, ϕ_2, and U are measured relative to the same reference electrode. The overpotential serves as the driving force for either the anodic or cathodic reaction, depending on if it is positive or negative. α_a and α_c represent the charge transfer coefficients. The R and T in Equation 3 represent the universal gas constant and the temperature respectively.

The charge balance for the electrode is shown in Equations 8 and 9.

$$a(Fj) = \frac{di_2}{dx} \quad (8)$$

$$-a(Fj) = \frac{di_1}{dx} \quad (9)$$

Where *a* represents the specific interfacial area between the electrode and electrolyte. The two equations are equal but opposite since the total current is equal to the sum of the current in the electrode and electrolyte.

The mass transport of lithium through the electrolyte is derived from concentrated solution theory where the driving force for mass transfer is the gradient in the electrochemical potential.[30] A binary electrolyte has three species, but only two independent driving forces because of the Gibbs-Duhem relation. In this case for the lithium ion and for the phosphate ion. Because electroneutrality is assumed, the transport of the lithium and phosphate ions are intrinsically related. The DFN model only uses an equation for the flux of the lithium ions while the phosphate ions transport is known because of electroneutrality. The transport equation for lithium ions is shown in Equation 10.

$$N_{Li^+} = -D_{el_{eff}} \frac{dc_{el}}{dx} + i_2 \frac{t^+}{zF} \tag{10}$$

$D_{el_{eff}}$ represents the effective diffusivity of the salt that makes up the electrolyte ($LiPF_6$). t^+ represents the transference number of lithium, while z is the charge on the lithium ion. The effective electrolyte diffusivity is calculated the same way that the effective electrolyte conductivity was calculated. This is shown in Equation 11.

$$D_{el_{eff}}{}_i = D_{el} \frac{\varepsilon_i}{\tau_i} \tag{11}$$

Where the electrolyte diffusivity is multiplied by the porosity and divided by the tortuosity of the separator or electrode depending on the section of the battery. The i subscript in Equation 11 is to show that the effective electrolyte diffusivity value depends on the section of the battery. The effective electrolyte diffusivity in the separator is found by multiplying by the porosity and dividing by the tortuosity of the separator, while the effective electrolyte diffusivity in the electrode is found by multiplying by the porosity and dividing by the tortuosity of the electrode.

Fick's second law of diffusion is used to model the transport of lithium through the electrode particles. Equation 12 shows Fick's second law of diffusion for the radial direction of the particles.

$$\frac{\partial c_s}{\partial t} = D_s \left[\frac{\partial^2 c_s}{\partial r^2} + \frac{2}{r} \frac{\partial c_s}{\partial r} \right] \tag{12}$$

Where D_s represents the diffusivity of lithium through the electrode particles.

While there are other boundary conditions and equations, the outline above served to identify all of the necessary parameters to model the electrochemical behavior of the battery in the DFN model. Table 1 shows the parameters needed for the DFN model. The table shows which chapter in the thesis the estimate for each of the parameters listed in Table 1 is obtained. These parameter estimates can be put into a DFN model to simulate an electrochemical system.

Table 1 Doyle Fuller Newman Model Parameters

Property	Separator	Graphite Electrode	Electrolyte	Lithium Electrode
Thickness (m)	3	3	-	-
Porosity	3	3	-	-
Tortuosity	3	3	-	-
Particle Radius (m)	-	3	-	-
a (m^{-1})	-	3	-	-
Exchange Current Density (A/m^2)	-	4	-	4
Charge Transfer Coefficients	-	4	-	4
Conductivity (S/m)	-	3	4	-
Diffusivity (m^2/s)	-	4	3	-
Open Circuit Voltage	-	3	-	-
Maximum Lithium Concentration (mol/m^3)	-	3	-	-
t^+	-	-	3	-
Electrolyte Lithium ion Concentration (mol/m^3)	-	-	3	-

CHAPTER 3. BASELINE PARAMETERS

Baseline parameters refer to the geometric parameters that outline the dimensions for the model and the equilibrium voltage curve that determines the baseline voltage for the various polarizations of the cell. To determine these baseline parameters, and all other parameters for that matter, an experimental electrochemical system must be selected. For this study, a graphite electrode was placed vs lithium foil in a coin cell. The graphite electrode was obtained from MTI, part number bc-cf-241-ss-005. The active material was graphite with copper as the current collector and styrene butadiene rubber (SBR) and carboxymethylcellulose sodium (CMC) as the binder materials. The lithium foil was also obtained from MTI, part number EQ-Lib-LiC60-300. The electrolyte was a 1 M $LiPF_6$ Ethylene Carbonate/Diethyl Carbonate mixture (1:1 v/v) from Sigma-Aldrich, part number 746746. The separator used was Celgard 2325, which consists of a tri-layer of polypropylene, polyethylene, and polypropylene. The coin cell hardware was CR2032 SS-316 obtained from MTI with stainless steel spacers and springs (Belleville washers).

The coin cells were assembled in a glove box filled with argon. The graphite electrodes and the lithium foils were both punched out with a 7/16” punch. The lithium foil was first placed in the bottom of the coin cell hardware as the negative electrode after being brushed off to remove the oxide layer. This could be observed from the surface becoming shiny after brushing. Eighty microliters of electrolyte was placed on top of the lithium foil using a micropipette and then two Celgard separators were placed on top of the electrolyte. Eighty more microliters of electrolyte were then placed on the separators and the graphite electrode was placed face down on the electrolyte. Three metal spacers and one spring were

placed on top of the graphite electrode after which the coin cell was crimped using an MSK-110 hydraulic crimping machine from MTI. The coin cells were crimped to the same pressure each time using a red indicator on the crimper (approximately 1000 kgf/cm^2). Coin cells made using this procedure were found to have consistent results throughout the experimental process.

One of the first steps in characterizing the experimental system is to determine the theoretical capacity of the graphite electrode. Two methods were used to calculate the amount of graphite on the electrode which is used to calculate the theoretical capacity. MTI reported a loading of 80 g/m^2 of active material for the graphite electrode, which multiplied by the surface area of the electrode resulted in a weight of 7.76 mg of graphite. The graphite electrode was also weighed in lab to verify the surface loading reported by MTI. The weight of the current collector was found by removing the electrode material from the copper and weighing the copper in lab. Once the weight of the electrode material was known, it was multiplied by the percent active material reported by MTI which resulted in a weight of 7.65 mg of graphite. The experimental weight determined in the lab of 7.65 mg was used to calculate the theoretical capacity of the electrochemical system. The mass of the graphite is converted to moles of graphite using the molecular weight of carbon. The moles of lithium are calculated from the moles of graphite from the stoichiometry of the electrochemical equation shown in Equation 13.

$$Li^+ + 6C + e^- \rightarrow Li_xC_6 \tag{13}$$

The moles of lithium in the electrode can be multiplied by the theoretical capacity for lithium which resulted in a theoretical capacity for the experimental graphite electrode of 2.85 mAh.

The calculated theoretical capacity is used as a starting point for cycling half cells where the graphite electrodes are cycled against lithium counter electrodes. The experimental capacity is highly dependent on the voltage limits and C-rate selected for the cell. Cells were initially cycled at approximately C/30 (0.0001 A) to determine the experimental capacity. For the graphite half-cell, the cell was cycled between 1.2 V and 0.005 V five times. The voltage limits for graphite are important to avoid plating of lithium.[33] The experimental capacity was taken to be the average of each of the cells cycled. The first cycle of each cell was not used due to the higher capacity of the first cycle attributed to SEI growth and other phenomena unique to the first cycle, commonly called a formation cycle.[34] The experimental capacity on average was 2.3±0.02 mAh for the graphite half-cells.

Once cycling limits and the theoretical capacity are known, experiments can be performed to determine the equilibrium voltage vs. state of charge (SOC) for each electrode. SOC here uses the same definition as Equation 1 where 0% SOC refers to an unlithiated graphite electrode and 100% SOC refers to a fully lithiated graphite electrode. The Galvanostatic Intermittent Titration Technique (GITT) was used to measure the equilibrium voltage curve of graphite.[35] An example of a single GITT step is shown in Figure 3. A small current of approximately C/30 (0.1 mA) is applied to the battery for one hour and then the cell is allowed to rest for 24 hours. The voltage will stop changing once it reaches the equilibrium voltage as seen below in Figure 3 from when the voltage has

stopped changing with time. This process is repeated until the cell reaches the upper voltage limit of 1.2 V after the 24 hour rest. Then the GITT process was conducted in the same manner except a current of –C/30 (-0.1 mA) was applied for 1 hour followed by a 24 hour rest for each step. This process was repeated until the cell reached the lower voltage limit of 0.005 V after the 24 hour rest.

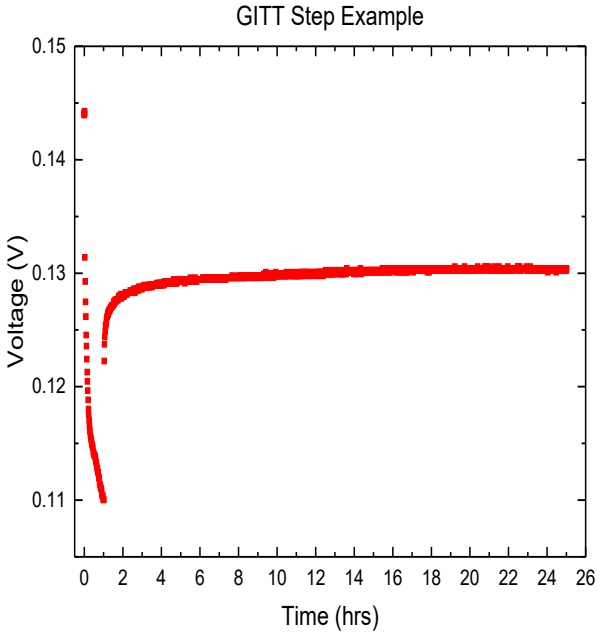

Figure 3 Example of the voltage response to one galvanostatic intermittent titration technique step.

The voltage values for the equilibrium voltage curve were taken to be the last reported voltage value for each 24 hour rest step. The SOC was calculated using coulomb counting after the initial SOC of the GITT cell was determined from comparing with GITT experiments using a fresh cell that started at 0% SOC. The results obtained for the graphite equilibrium voltage from the GITT experiments of six cells are shown in Figure 4.

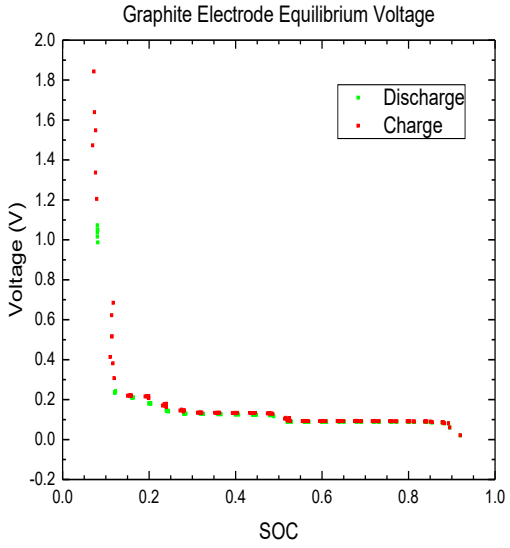

Figure 4 Equilibrium voltage of graphite from GITT Results. Values for charge and discharge are differentiated to show the hysteresis between charge and discharge values.

The graphite material used exhibited hysteresis where the equilibrium voltage curve measured during GITT charging and discharging differed. Other researchers have also reported hysteresis when looking at the equilibrium voltage curve for graphite electrodes.[36] Because each of the cells was cycled in the same manner prior to initiating the GITT experiments the initial voltages before starting the GITT discharge are very similar. The voltage values, at the end of charging, vary more than the initial voltages before discharging. To see if this is because of the GITT starting point, GITT could be conducted on cells that initially begin at fully discharged for the experimental cycling procedure outlined to compare with the results shown here. Figure 5 shows that there is hysteresis throughout the whole equilibrium voltage curve. Though it is not as drastic as seen in the 0-0.1 SOC range.

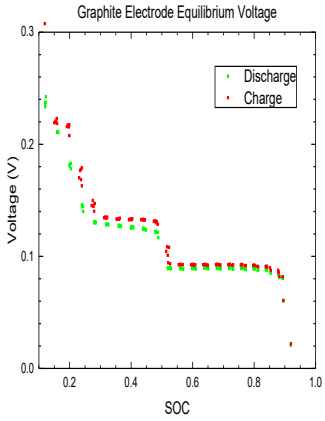

Figure 5 Close up of Figure 4 to better illustrate hysteresis between 0.2 and 1.0 SOC.

The final equilibrium voltage curve estimate was taken to be the average of the charge and discharge GITT results and is shown in Figure 6. The average equilibrium voltage vs SOC was determined by fitting an equation to the GITT results. The equilibrium voltage curve is the starting point for any calculation so the fit obtained should be as close to possible to the experimental data. The equation used for the equilibrium voltage of the graphite electrode in the DFN model is shown in Equation 14.

$$\begin{aligned} &5.1\tanh\left(-26.2\left(\frac{c_s}{c_{s,max}}\right)+0.953\right) \\ &\quad+0.0453\tanh\left(-23.1\left(\frac{c_s}{c_{s,max}}\right)+5.11\right) \\ &\quad+0.0197\tanh\left(-51.9\left(\frac{c_s}{c_{s,max}}\right)+26.1\right) \\ &\quad-0.0448\tanh\left(49.4\left(\frac{c_s}{c_{s,max}}\right)-44.8\right)+5.19 \end{aligned} \tag{14}$$

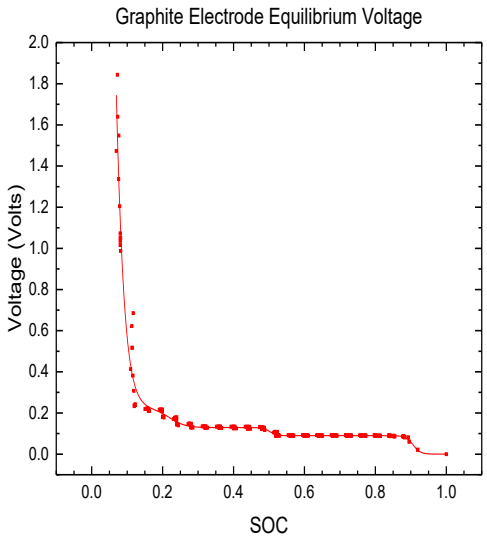

Figure 6 The results for each step of the galvanostatic intermittent titration technique graphed versus state of charge. The line represents an equation used to fit the galvanostatic intermittent titration techniques results for inputting the graphite equilibrium voltage into the model.

To outline the physical space of the DFN model, geometrical parameters are needed. The thicknesses of the graphite electrode and the separator were provided by the suppliers. The thickness of the separator is 0.025 mm, and the thickness of the graphite electrode and current collector is 0.05 mm. To obtain the thickness of the graphite electrode, the thickness of the copper current collector supplied by the supplier, 0.009 mm, was subtracted from the total thickness. This resulted in a thickness of 0.041 mm for the graphite electrode. The thickness of the graphite electrode was verified from the SEM image shown in Figure 7.

The particle radius of the graphite electrode was estimated by taking the average of the diameters measured from an SEM image. Though the average radius was used in this

thesis, and is commonly used in many papers, the author acknowledges that this can introduce some error into the system as opposed to using a distribution of radii in the model.[37] The SEM image was taken by a fellow lab member and is shown in Figure 7. The diameters were measured as the longest distance spanned by the particle, since they are not spherical in shape. The diameters' measurements were taken using the imaging software Image J. The average particle diameter measured from the SEM image was 17 μm. This gives a particle radius of 8.5 μm.

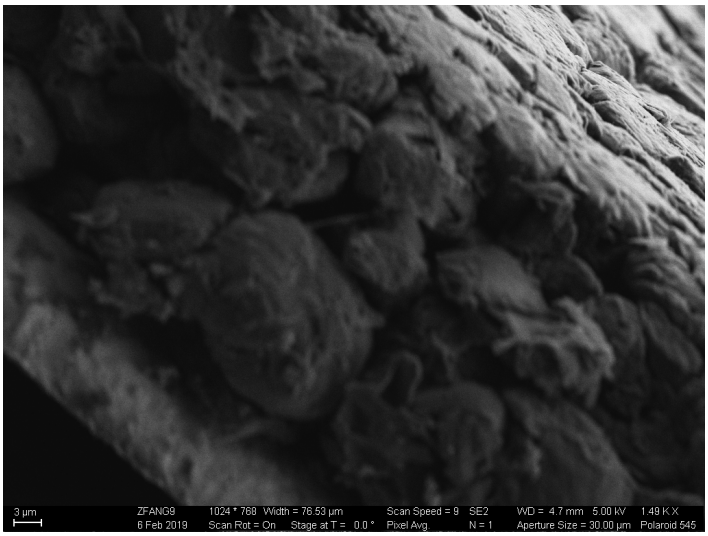

Figure 7 Scanning electron microscope image of a pristine graphite electrode used for estimating the particle diameter. Imaging was done by Jung Fang, a member of Dr. Fuller's lab.

One other geometrical parameter that is needed for the model is the specific interfacial area. The specific interfacial area is the ratio of the surface area that is shared by the electrode and the electrolyte to the superficial volume of the electrode. One challenge with modeling porous electrodes is determining the specific interfacial area. One way to estimate the specific interfacial area is to assume spherical particles.[38] The process

for estimating the specific interfacial area assuming spherical particles is outlined as follows. Equation 15 defines the specific interfacial area, a.

$$a \equiv \frac{\text{interfacial area}}{\text{superficial volume}} \tag{15}$$

The interfacial area is the surface area of the electrode spheres in contact with the electrolyte. This can be found by estimating the total number of spheres and then multiplying by the surface area for each individual sphere. Equation 16 estimates the number of spheres in the electrode based on the solid phase fraction, the superficial volume, and the volume of a single sphere.

$$\text{number of spheres} = \frac{V(1-\varepsilon)}{{}^{4}/_{3}\,\pi r^{3}} \tag{16}$$

Equation 17 shows the number of spheres equation multiplied by a single sphere's surface area substituted in for the interfacial area.

$$a = \frac{\frac{V(1-\varepsilon)}{{}^{4}/_{3}\,\pi r^{3}} 4\pi r^{2}}{V} \tag{17}$$

Equation 18 shows the final simplification for estimating the specific interfacial area of the electrode.

$$a = \frac{3(1-\varepsilon)}{r} \tag{18}$$

The porosity of the separator was provided by the manufacturer and was listed as 0.39. The porosity of the electrode can be determined using Hg-porosimetry. Lacking the experimental capabilities to measure the porosity of the graphite electrode, values were taken from the literature. The porosity of commercial graphite electrodes from two different sources were measured using Hg-porosimetry in two separate papers. The reported porosities were 0.292 and 0.329.[20,22] This thesis used an average of the two reported values for the initial estimate for the graphite electrode porosity. Other parameters were also determined from the literature since the equipment to experimentally measure the values was unavailable. The effective conductivity for a thin film graphite electrode is measured as 3000 S/m using a four point probe method.[39-40] The transference number of lithium was reported to be 0.162 for a 1 M $LiPF_6$ ethylene carbonate diethyl carbonate (1:1 w/w) at 25° C.[41] The diffusion coefficient of the lithium salt in a 1 M $LiPF_6$ ethylene carbonate/diethyl carbonate (1:1 w/w) was reported to be 1.2×10^{-9} m^2/s at 25° C.[42]

This chapter estimated each of the baseline parameters using GITT, SEM images, and information reported by the electrode manufacturer. Other parameters, not measured in this thesis, were estimated using literature values. These baseline parameters will be put into the DFN model to outline the geometry of the experimental system being modeled as well as establishing the equilibrium voltage curve for the graphite electrode. Parameters used to calculate the voltage polarizations from the equilibrium voltage curve are estimated in the next chapter from electrochemical impedance spectroscopy (EIS) data.

CHAPTER 4. ELECTROCHEMICAL IMPEDANCE SPECTROSCOPY PARAMETERS

Now that the baseline parameters have been estimated in the previous chapter, the parameters needed to calculate the polarizations of the cell will be estimated in this chapter. Electrochemical impedance spectroscopy (EIS) is a popular experimental technique used to characterize the impedance of a cell because it is non-invasive and, in theory, can separate the different impedances experienced by the cell by the different time constants associated with them. For example, low frequency impedance is associated with the mass transport polarization of the cell because the time constant for the mass transport polarization is usually much longer than the time constants associated with the kinetic/double-layer charging, or ohmic polarizations. EIS spectra were taken after each step of the GITT process for the graphite vs. lithium coin cells. The GITT process used was the same as outlined in Chapter 3 where the cell was discharged at approximately C/30 (0.0001 A) for one hour and then allowed to rest for 24 hours. EIS was conducted using a Metrohm potentiostat using a frequency range from 100 kHz to 0.01 Hz. A 5 mV perturbation was applied around the open-circuit voltage of the cell at each SOC. Five points were sampled for every decade of frequency. An example of the EIS results is shown in Figure 8.

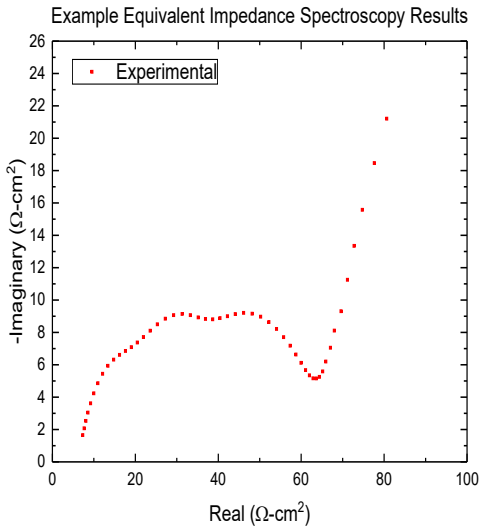

Figure 8 Electrochemical impedance spectroscopy results example for the coin cell at 0.181 V.

EIS spectra, like other electrochemical experimental data, are often fit by models. In this thesis, an equivalent circuit model was used. As explained in Chapter 1, an equivalent circuit model uses common circuit elements to represent the underlying electrochemical system. Circuit elements are selected to represent the ohmic, charge transfer, and mass transport polarizations. Additionally, circuit elements are included to represent the double layer. The double layer is a thin film of ions that builds up on the interface between the electrode and the electrolyte. Chapter 1 mentions that in the DFN model in this thesis the double layer is not modeled as its effects are only seen on the order of milliseconds. Since EIS spectra cover a wide range of time scales, the double layer needs to be modeled here to paint a more complete picture of the different impedance elements present in the cell. The equivalent circuit used to fit the experimental data is shown in Figure 9. This equivalent circuit was selected based on the appearance of the EIS data and

the elements in the cell. From the literature, a similar equivalent circuit has also been used by Mendoza-Hernandez et al. when fitting EIS data from a graphite electrode.[43-44]

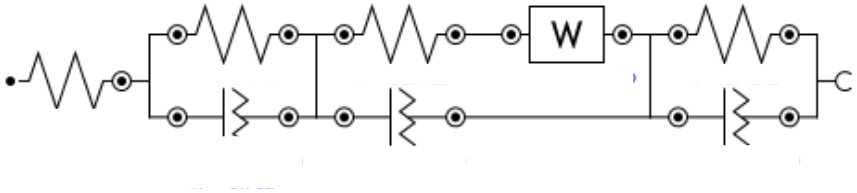

Figure 9 Example of the equivalent circuit used to fit the experimental electrochemical impedance spectroscopy results.

These circuit elements all represent different parts and physics of the cell. The resistor on the far left represents the ohmic resistance, which is used to model the ohmic polarization. The subsequent resistor is in parallel with an element called a constant phase element (CPE). The equivalent circuit uses CPEs in the place of capacitors to represent the double layer. EIS usually have depressed semicircles where equivalent circuits using capacitors have true semicircles. Because of this, CPEs are used in equivalent circuits to better fit experimental EIS data.[45] The equation for the impedance of a CPE is shown in Equation 19.

$$\frac{1}{Z_{CPE}} = Y(j\omega)^N \tag{19}$$

Where Z_{CPE} represents the impedance of the CPE, Y represents the admittance when ω is equal to one, j is the square root of -1, ω represents the frequency, and N represents the CPE exponent. The equation for the impedance of a CPE is equivalent to the equation for the impedance of a capacitor when N equals one. The resistors in parallel with the CPEs

represent the charge transfer resistance while the CPEs represent the double layer capacitance. The final part of the circuit includes a resistor in series with a Warburg impedance in parallel with a CPE. The Warburg impedance represents the mass transport polarization.

Fitting the EIS data to the equivalent circuit was done using PyCharm, an integrated development environment for python. The program used was an open source Python module for fitting EIS data begun at the Electrochemical Society 2018 hack week intended to make EIS fitting more intuitive and reproducible.[46-47] The fitting software used a semi-infinite Warburg impedance shown in Equation 20.

$$Z_W = \sigma\omega^{-0.5}(1-j)\tanh\left(\delta\left(\frac{j\omega}{D}\right)^{0.5}\right) \tag{20}$$

Where σ represents the Warburg coefficient, δ represents the Nernst diffusion layer thickness, and *D* represents an average value of the diffusion coefficients of the diffusing species. *j* is again the square root of -1 and ω is the frequency. A semi-infinite Warburg impedance is used because the separator is not infinitely thick. An example of the fit obtained from PyCharm is shown in Figure 10.

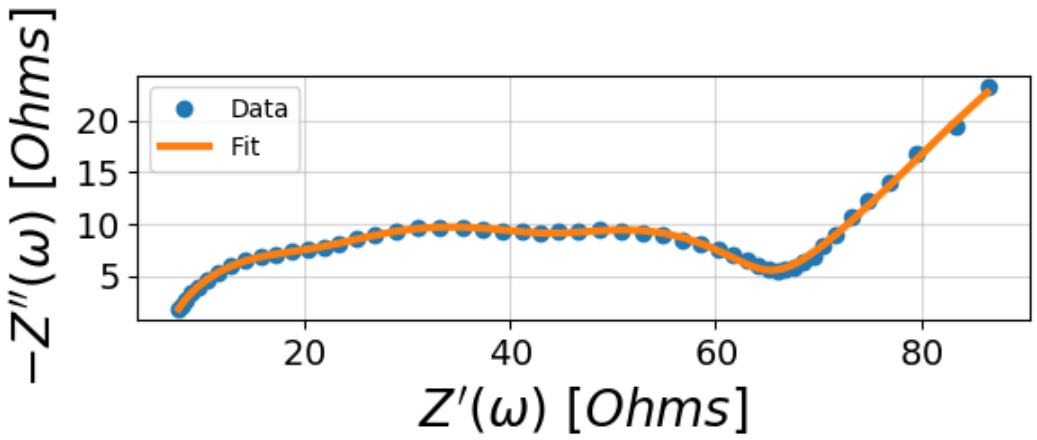

Figure 10 Example PyCharm fitting of graphite EIS data.

The first resistor in the equivalent circuit from Figure 9 represents the ohmic resistance of the cell. The resistance value of the resistor being the estimated ohmic resistance from the equivalent circuit fitting. The ohmic polarization is a result of the voltage loss associated with moving ions to pass current through the cell. Ohm's law, shown in Equation 3 in Chapter 2, shows that the ohmic voltage loss is a function of the amount of current as well as the conductivity of the electrode and the electrolyte. Assuming that the conductivity of the electrode is orders of magnitude greater than the electrolyte conductivity, the ohmic resistance can be used to estimate the electrolyte conductivity, as shown in Equation 21.

$$R_{ohmic} = \frac{L}{\kappa_{eff} A} \tag{21}$$

Where L represents the thickness of the separator, κ_{eff} is the effective conductivity, shown in Equation 22, and A is the geometric area of the electrode-electrolyte interface.

$$\kappa_{eff} = \kappa\frac{\varepsilon}{\tau} \tag{22}$$

The effective conductivity is the conductivity multiplied by the porosity, ε, and divided by the tortuosity, τ, of the separator. Since it was assumed that the electrode conductivity was much greater than the electrolyte conductivity the ohmic resistance is only measuring the electrolyte conductivity in the separator as in the electrode only a negligible amount of current passes through the electrolyte.

While the porosity of the Celgard 2325 separator is reported by the manufacturer to be 0.39, the tortuosity is not reported. T. Joshi, a previous member of Dr. Fuller's group, measured the tortuosity of the separators by measuring how the high frequency impedance of experimental EIS data changed with an increasing number of separators in a conductivity cell.[48] Using an electrolyte of known conductivity, EIS was measured for five different conductivity cells to find the high frequency impedance. The conductivity cells each contained a different number of separators from 1-5. The tortuosity calculated from each of the cells was taken and averaged for a final value of 4.11. Using this value, the electrolyte conductivity can be estimated from the high frequency impedance, or ohmic resistance, of the cell.

The estimated value for the ohmic resistance was 6.4 Ω-cm^2 taken as the average for the resistance of the ohmic resistor from all the equivalent circuits used to fit the EIS

data for all of the cells. The estimated value for the ohmic resistance was used to calculate an effective conductivity of 0.078 S/m using Equation 21. The conductivity was then calculated from Equation 21 using the previous values for the porosity and tortuosity. This yielded the conductivity of the electrolyte to be 0.82 S/m. This value was the same as the literature value of 0.82 S/m.[49]

The effective electrolyte conductivity is different in the porous electrode than in the separator due to different values for the porosity and tortuosity. Since the tortuosity of the graphite electrode is unknown, the Bruggeman relationship was assumed. The Bruggeman relationship assumes that the tortuosity is equal to the inverse square root of the porosity.[50] Other papers have left the tortuosity as a fitting parameter, but this thesis elected to use the Bruggeman relationship to eliminate one additional parameter.[51] If this relationship had been used for the separator, the tortuosity would have been 1.6 as compared to 4.11 found experimentally. This shows that the Bruggeman relationship, in the case of the separator, is not a good assumption for the tortuosity. However, the Bruggeman relationship is commonly used to estimate tortuosity. One other method that has recently been explored in our group is the use of FIB-SEM to construct an image of an electrode to better estimate the porosity and tortuosity of the material in question.[52] This method could be used to obtain a more accurate, experimentally obtained estimate for the porosity and tortuosity of the graphite electrode.

The exchange current densities for the graphite and lithium electrodes were also obtained from the EIS spectra of the graphite vs. lithium coin cells. The exchange current densities were estimated from the resistors representing the charge transfer resistances for the lithium electrode, the graphite electrode, and the SEI. At each of these interfaces,

electrochemical reactions are occurring where lithium ions and electrons are reacting. Each of these electrochemical reactions is associated with a resistance that is termed a charge transfer resistance. The equation used to represent the charge transfer resistance from the Butler Volmer equation used in this model is shown in Equation 23.

$$R_{ct} = \frac{RT}{\alpha z F j_0 a V} \tag{23}$$

Where R represents the universal gas constant, T the temperature, α the charge transfer coefficient, z the charge of the ion in the electrochemical equation, F the Faraday constant, j_0 the exchange current density, a the specific interfacial area, and V represents the volume.

To be able to estimate the exchange current density for each element represented by the equivalent circuit, each circuit element must first be assigned to a corresponding part of the coin cell. In the equivalent circuit, there are two parallel resistor-CPE pairings in series. These in turn are in series with a resistor in series with a Warburg impedance all in parallel with a CPE. Initially, it was thought that the resistor and CPE associated with the Warburg impedance would represent the graphite electrode, which has mass transport limitations. The two RC circuits without the Warburg impedance would then represent the Solid Electrolyte Interphase (SEI, a layer that grows on the surface of the graphite electrode due to a side reaction between the electrolyte and the graphite electrode), and the lithium foil. However, similar fits were obtained independent of which resistor and CPE values were associated with the Warburg impedance. An example of this is shown in Figure 11.

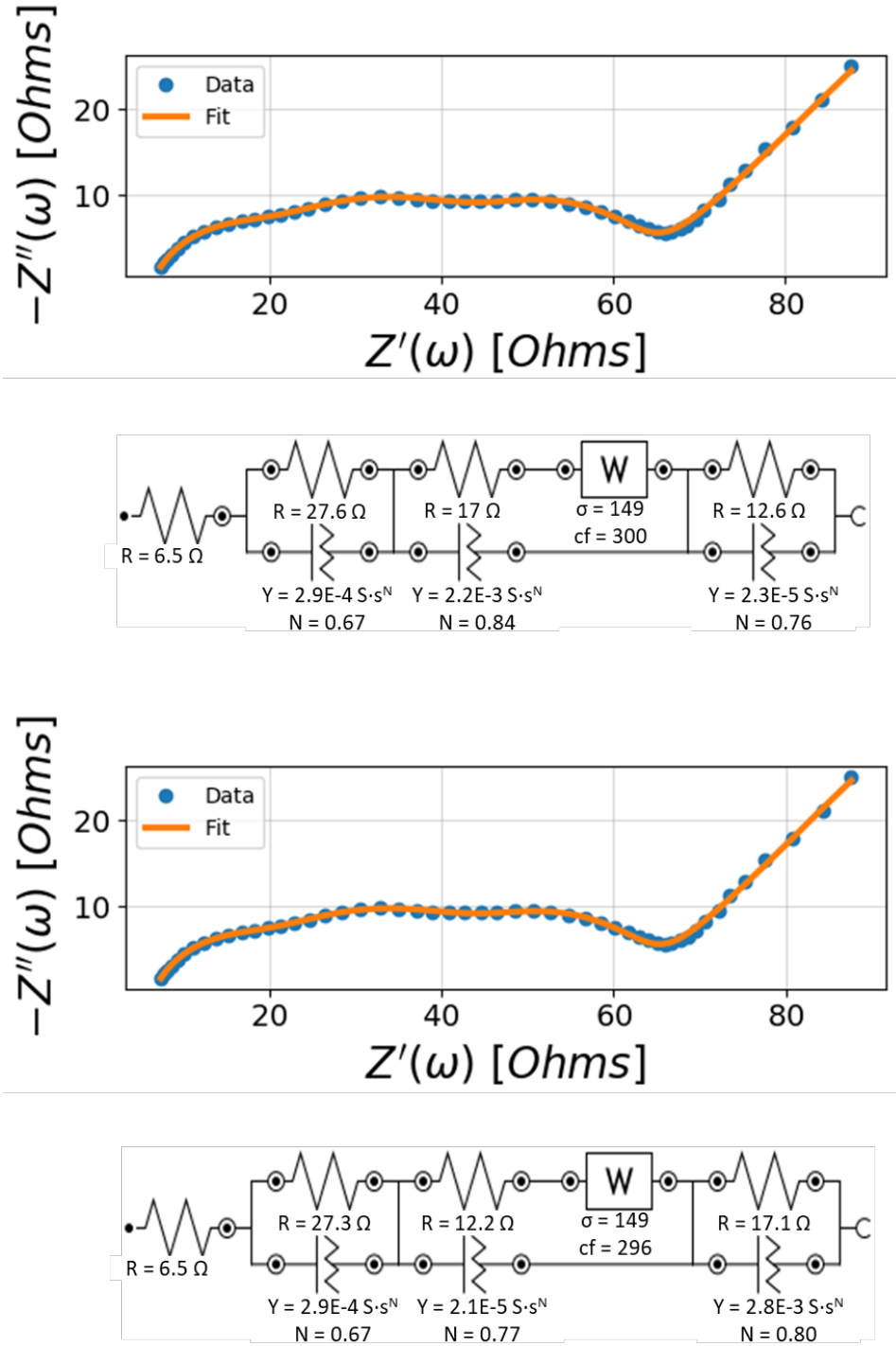

Figure 11 Graphs to show the interchangeability of the resistor-CPE pairs. The top graph shows the original fit obtained for the EIS data taken at 127 mV. The bottom graph shows the fit obtained for the EIS data when the last resistor-CPE pair is switched with the second resistor-CPE pair. Even though this changes the resistor-CPE pair associated with the Warburg impedance, the fit obtained is nearly identical.

Figure 11 shows that the fit obtained is similar when the resistor-CPE pairing associated with the Warburg impedance in the initial fit is switched with the last resistor-CPE pairing from the original fit. The cf term in the figure references the hyperbolic tangent term from Equation 20 that is used as a correction factor to change the Warburg impedance from an infinite diffusion layer to a semi-infinite diffusion layer.

Figure 12 shows that a similar fit was also obtained when placing the Warburg impedance in series with all the other circuit elements.

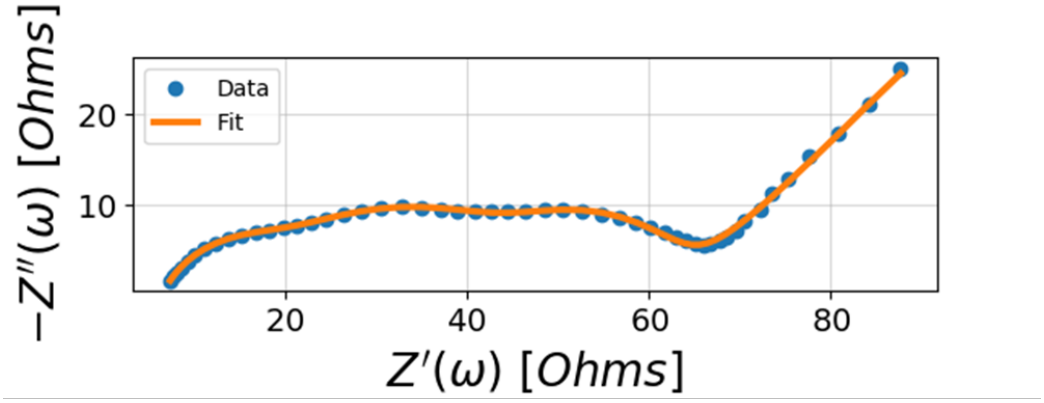

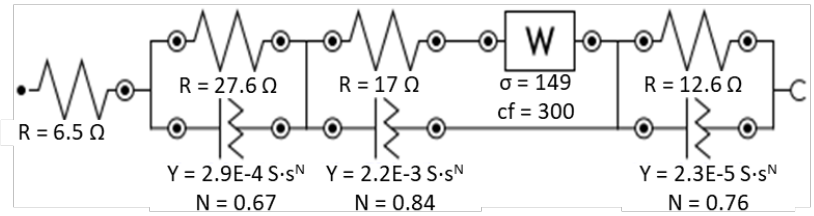

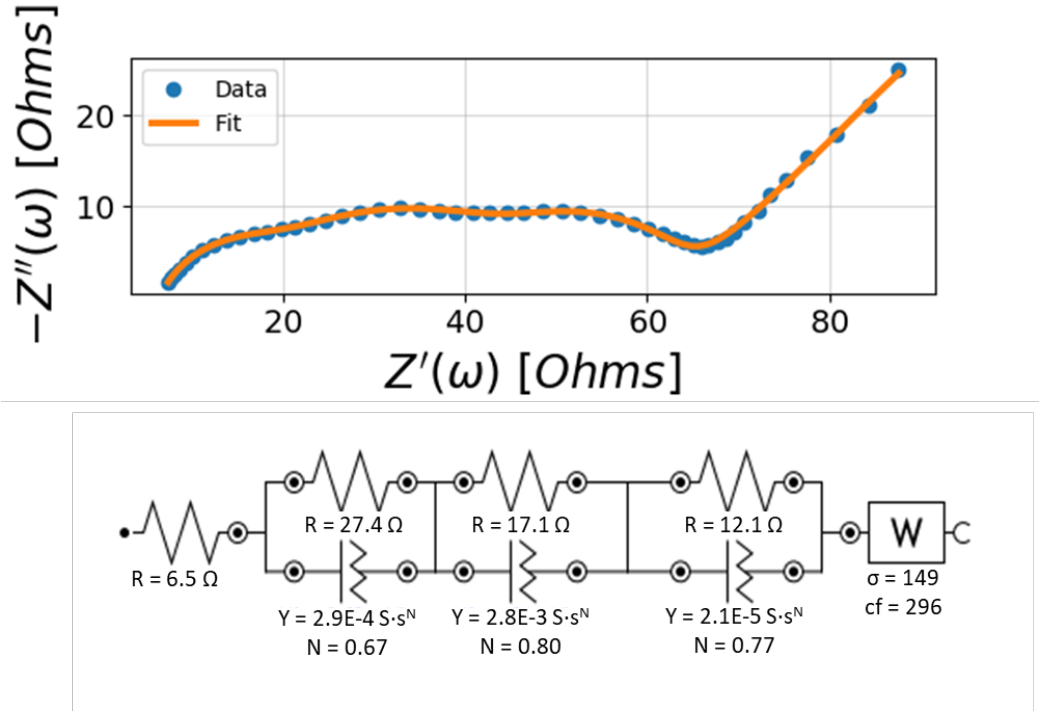

Figure 12 Graphs to show that the Warburg impedance can be associated with a resistor-CPE pair in the circuit or placed on its own outside the circuit with minimal effect. The top graph shows the original fit obtained for the EIS data taken at 127 mV. The bottom graph shows the fit obtained for the EIS data when the Warburg impedance is moved to be in series with all of the circuit elements instead of in a resistor-CPE pairing.

Because the EIS fitting was independent from the position of the Warburg impedance, the resistor-CPE pairing associated with the Warburg impedance could not be assigned to the graphite electrode as initially assumed. Other assumptions will be made to assign each circuit element to a component of the electrochemical system.

While the resistance and capacitance of the three resistor-CPE pairings were interchangeable, the resistance and CPE values would consistently appear as the same pairs. Because of the consistent pairings, the resistor-CPE pairings were able to be consistently identified throughout the EIS data gathering. Because the lithium foil charge transfer resistance should not be SOC dependent, it was assumed that the only charge

transfer resistance that was not SOC dependent corresponded to the lithium foil. Ideally, the SEI and graphite resistor-CPE pairings would also be identified and separated. However, since the SEI layer is not included in this model, the charge transfer resistances for the SEI and the graphite electrode are added together in the model to estimate the total charge transfer resistance for the graphite electrode. The lumped exchange current density value made differentiating the resistor-CPE values for the graphite electrode and the SEI not necessary for the calculation of the charge transfer estimate for the model. The values for the charge transfer resistances for the lithium electrode and the SEI and graphite electrode are shown in Figures 13-14.

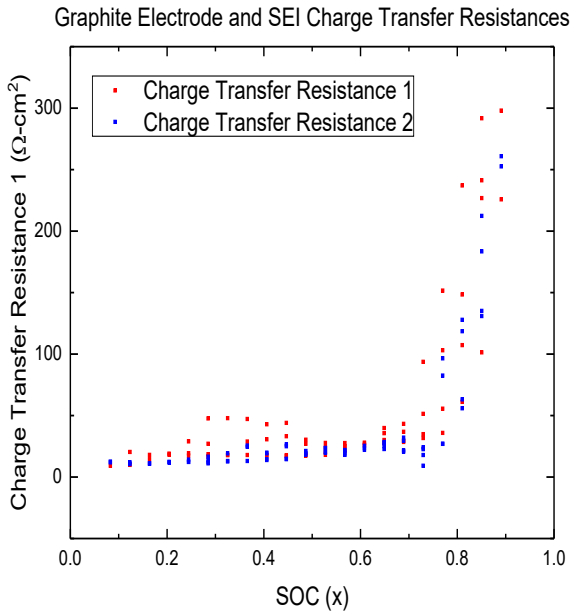

Figure 13 Charge transfer resistance values from EIS fitting associated with the SEI and the graphite electrode. They are added together to sum to one total charge transfer resistance in the model.

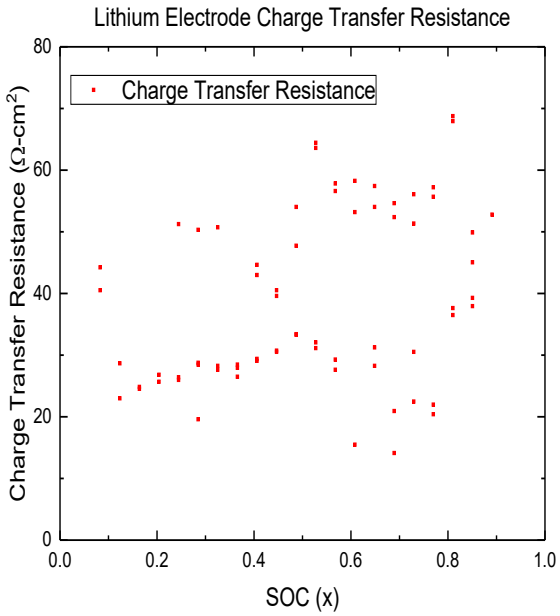

Figure 14 Charge transfer resistance values from EIS fitting associated with the lithium electrode.

An average value was used for the charge transfer resistance for the lithium electrode since it is assumed to be independent of SOC. The average value for the charge transfer resistance was 38.9 Ohm-cm^2. The graphite electrode and SEI charge transfer resistances were added together as the SEI layer is not included in the model. The exchange current density can be calculated from the charge transfer resistance by rearranging Equation 23 as shown in Equation 24.

$$j_0 = \frac{RT}{\alpha z F R_{ct} a V} \tag{24}$$

The estimate for the exchange current density for the lithium electrode was 14 A/m^2. The estimate for the exchange current density for the graphite electrode, along with the linear fit used to input the exchange current density into the model, is shown in Figure 15.

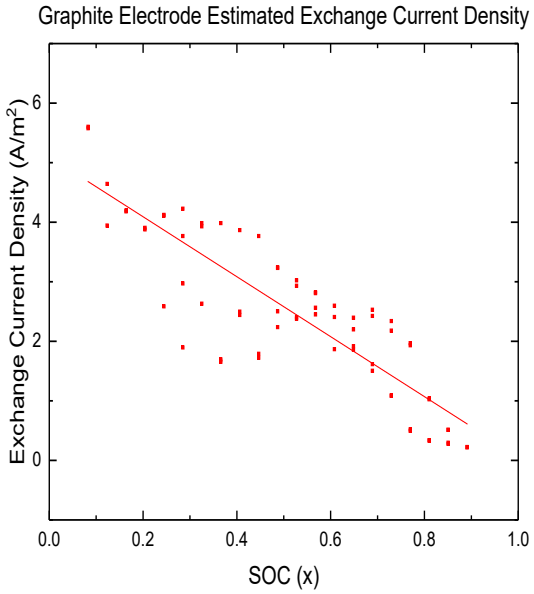

Figure 15 Estimated exchange current density for the graphite electrode vs. SOC. The linear fit used to input the estimated exchange current density as a function of SOC into the model is also shown.

The equation used in the model for the graphite exchange current density is shown in Equation 25.

$$2.3 - 2.26(SOC) \tag{25}$$

In the literature, the exchange current density is sometimes fit to an equation that dictates it be 0 when the cell is fully lithiated or unlithiated.[22] This is because of the fact that the kinetics are dependent on the concentration of the reactants. When the cell is

completely lithiated, no more lithium can intercalate into the graphite electrode. When the cell is completely unlithiated no lithium can be oxidized from the graphite electrode. These are factors that affect the current passing through the cell. However, the exchange current density is a measure of the equilibrium that exist between oxidation and reduction at an electrode's surface. In other words, the exchange current density is a measure of both the rate of oxidation and reduction when the cell is at equilibrium. Even when the cell is not passing any current, there is still oxidation and reduction happening at the surface of both electrodes. This is what the exchange current density is measuring. Even when the electrode is completely lithiated or unlithiated there is still reduction and oxidation happening at equilibrium. The exchange current density is a measurement of that rate and is not zero even when the cell is completely lithiated or unlithiated. However, the exchange current density would be zero if the lithium concentration in the electrode and the electrolyte were zero as there would be no lithium ions to reduce and oxidize at the electrode's surface.

The diffusivity for lithium in the solid phase of the graphite electrode was also estimated from the EIS spectra using Equation 26.[54-55]

$$D_{\mathrm{Li}^+} = \frac{1}{2}\left(\frac{\frac{dE}{dx}V_M}{\sigma_W F a V}\right)^2 \tag{26}$$

Where $\frac{dE}{dx}$ is the slope of the equilibrium voltage curve vs. x, σ_W is the Warburg coefficient, V_M is the molar volume of graphite, F is Faraday's constant, a is the specific interfacial area, and V is the volume.

One cause for concern from using Equation 26 to estimate the effective solid phase diffusivity for graphite specifically is the large sections of the equilibrium curve that are flat.[56] For reference, the equilibrium voltage curve vs. SOC for graphite is provided again in Figure 16.

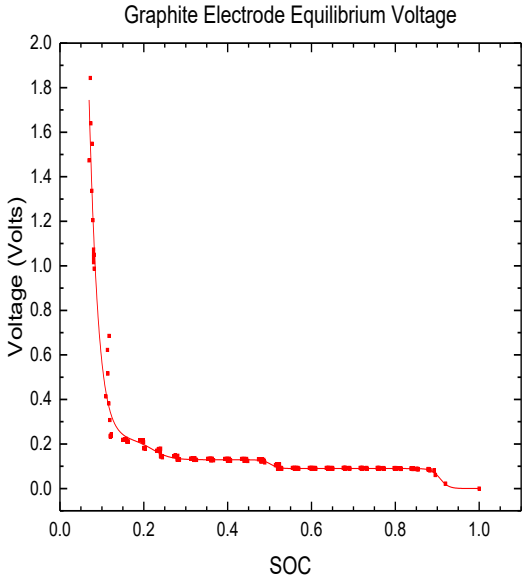

Figure 16 Graphite electrode equilibrium voltage curve provided to show regions where the curve is flat.

In Figure 16 the equilibrium voltage curve is flat between SOCs 0.3 and 0.45, and between SOCs 0.55 and 0.85. Using Equation 26, areas where the equilibrium voltage curve is flat gives values of diffusivity that are orders of magnitude smaller.[20] This thesis follows a similar approach to Schmalstieg et al. where estimated diffusivity values are only considered for regions where the equilibrium voltage curve is not flat.

Referring again to Equation 26, values must be obtained for $\frac{dE}{dx}$ and σ_w. $\frac{dE}{dx}$ is the slope of the equilibrium voltage curve at the SOC the EIS data was taken. To find the slope

of the equilibrium voltage curve at each SOC, the derivative of the equation used to fit the equilibrium voltage curve was taken and evaluated at the appropriate SOC. The SOC was obtained from counting coulombs from each GITT step taken between the EIS experimental data sets. Figure 17 shows $\frac{dE}{dx}$ for each set of EIS data.

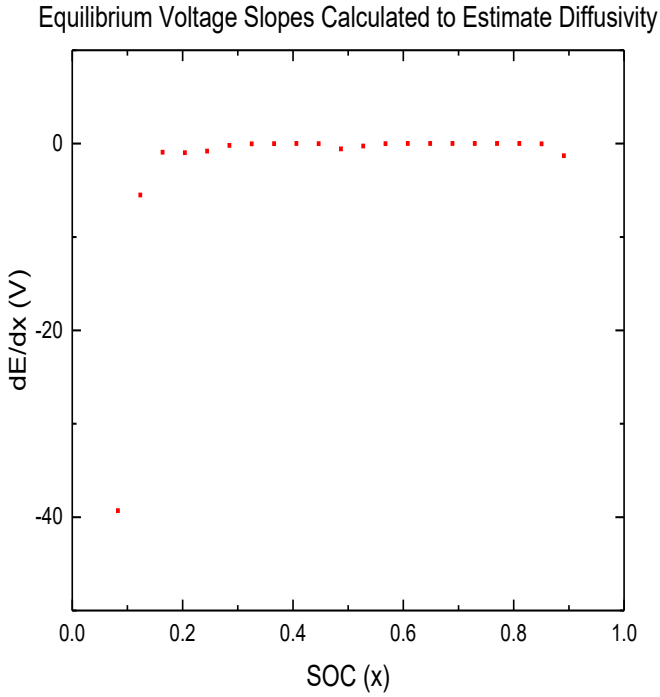

Figure 17 Equilibrium voltage curve slopes determined by taking the derivative of the equation used to fit the equilibrium voltage curve at the SOC of each set of EIS data. These slopes are used in Equation 26 to estimate the solid phase diffusivity of graphite.

As mentioned previously, the slopes from where the equilibrium voltage curve is flat were not used to estimate the solid phase diffusivity. It was visually determined to be SOCs between 0.3 and 0.45 and SOCs between 0.55 and 0.85.

σ_w is the Warburg coefficient and is determined by finding the slope of the real or imaginary impedance against the inverse square root of frequency of the EIS data in the

Warburg region. The Warburg region is characterized by a straight line on a Nyquist plot, which plots the imaginary impedance vs. real impedance. Figure 18 shows examples of the real impedance and the imaginary impedance being graphed against the inverse square root frequency along with linear fits used to calculate the slopes used for the Warburg coefficients.

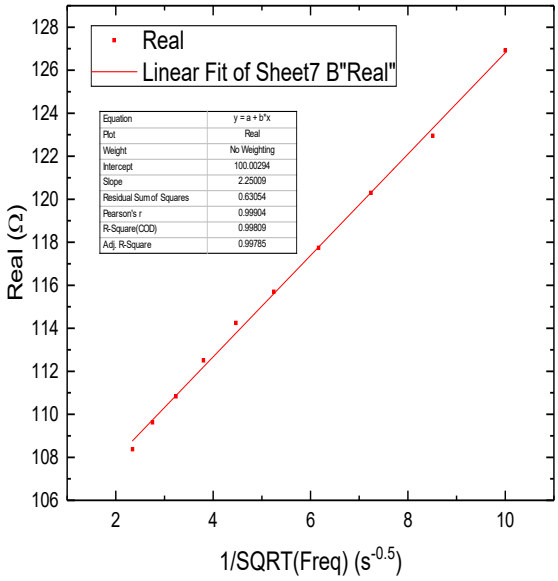

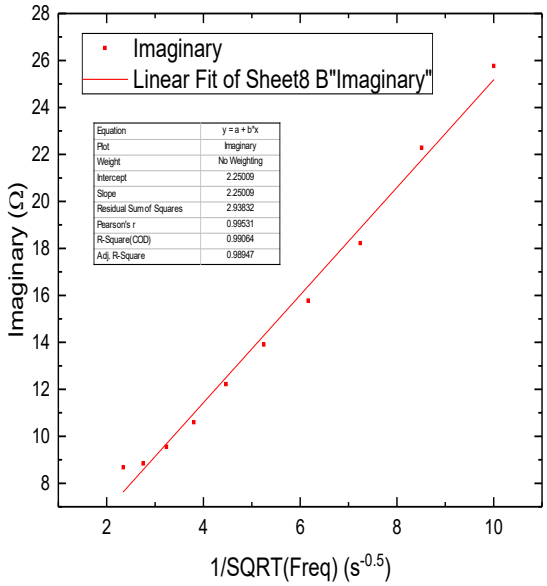

Figure 18 Example of real (top graph) and imaginary (bottom graph) impedances graphed against the inverse square root of frequency of EIS data taken at a SOC of 0.325.

The average of the slopes from the real and imaginary impedance vs the inverse square root of frequency was used as the Warburg coefficient to estimate the solid phase diffusivity of graphite from Equation 26. The estimate for the solid phase diffusivity of graphite is shown in Figure 19 along with the exponential equation fit used to input the estimate into the gPROMs model. The equation used in the model for the solid phase diffusivity of graphite is shown in Equation 27.

$$6.06 \times 10^{-17} e^{\left(-\frac{SOC}{0.0286}\right)} + 4.74 \times 10^{-15} \tag{27}$$

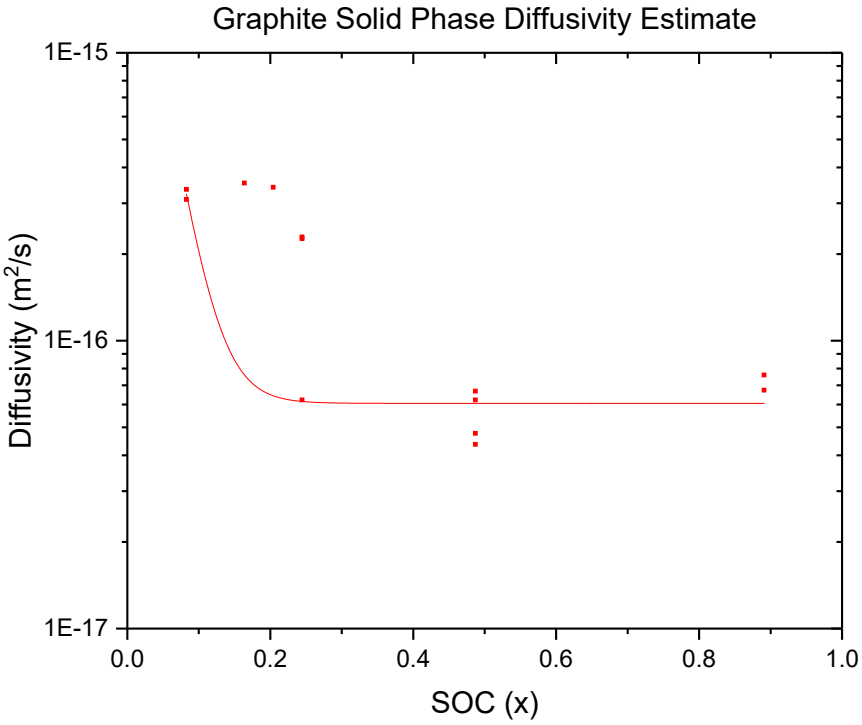

Figure 19 Graphite solid phase diffusivity values estimated from EIS data using Equation 26. Also including the equation fit used to input the estimate into the gPROMs model.

The fit shown above was used because it was similar to the fit obtained by Schmalstieg et. al.[20]

CHAPTER 5. COMPARING EXPERIMENTAL AND SIMULATION DISCHARGE CURVES

Now that estimates have been obtained for all of the parameters needed for the DFN model, simulation results using the parameter estimates will be compared to experimental discharge data. Table 2 compiles the parameter estimates obtained in this thesis. The parameter estimates in Table 2 were put into a DFN model coded in gPROMS, and the simulation results were compared to experimental discharge data for the graphite vs. lithium coin cells. Coin cells were manufactured using the materials listed in Chapter 3 in a glove box and cycled on an Arbin cycler. Cells were discharged at 0.1 mA, 0.2 mA, 0.4 mA, 0.67 mA, and 1 mA These rates were between C/30 and C/2 with the C-rates being determined based on 2.85 mAh, the theoretical capacity calculated in Chapter 3. The simulation results for a 0.1 mA discharge are compared to the experimental data for the graphite vs lithium coin cell in Figure 20.

Table 2 Compiled Estimates for Doyle Fuller Newman Model Parameters

Property	Separator	Graphite	Electrolyte	Lithium
Thickness (μm)	50 [p]	41 [p, SEM]	-	-
Porosity	0.39 [p]	0.31[l]	-	-
Tortuosity	4.11 [m]	1.5 [c]	-	-
Particle Radius (μm)	-	8.5 [SEM]	-	-
Specific Interfacial Area (m^{-1})	-	110000 [c]	-	-
Exchange Current Density (A/m^2)	-	Figure 15 [EIS]	-	14 [EIS]
Charge Transfer Coefficients	-	0.5, 0.5 [a]	-	0.5, 0.5 [a]
Conductivity (S/m)	-	3000 [l]	0.82 [EIS]	-
Diffusivity (m^2/s)	-	Figure 19 [EIS]	1.2E-9 [l]	-
Equilibrium Potential	-	Figure 6 [GITT]	-	-
Maximum Lithium Concentration (mol/m^3)	-	39000 [c]	-	-
Transference Number	-	-	0.173 [l]	-
Electrolyte Concentration (mol/m^3)	-	-	1200 [p]	-
p-provided by manufacturer, SEM – scanning electron microscope, l-literature, m-measured, c-calculated, EIS-electrochemical impedance spectroscopy, a-assumed, GITT-galvanostatic intermittent titration technique				

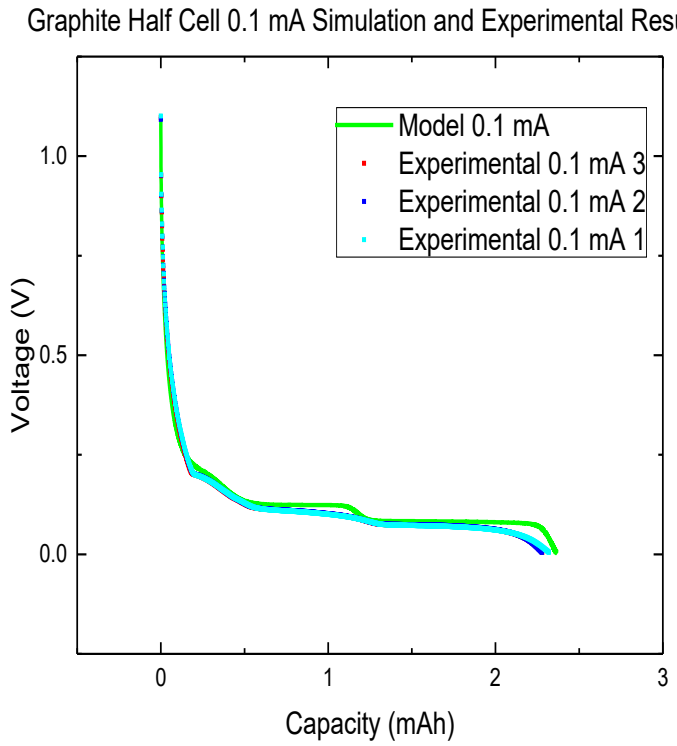

Figure 20 Simulation and experimental discharges for graphite vs. lithium coin cells at 0.1 mA.

The simulation results show good agreement with the experimental data taken at 0.1 mA. The main difference being the two voltage plateaus lasting longer for the simulation results than for the experimental data. The simulation capacity at 0.1 mA was 2.37 mAh while the average experimental capacity was 2.28 mAh.

The results at such a slow C-rate (approx. C/30) is a good means of analyzing the Equilibrium Voltage vs. SOC curve used for the model. Figure 21 adds in the GITT data and equilibrium voltage curve to Figure 20 to compare with the experimental data and simulation results.

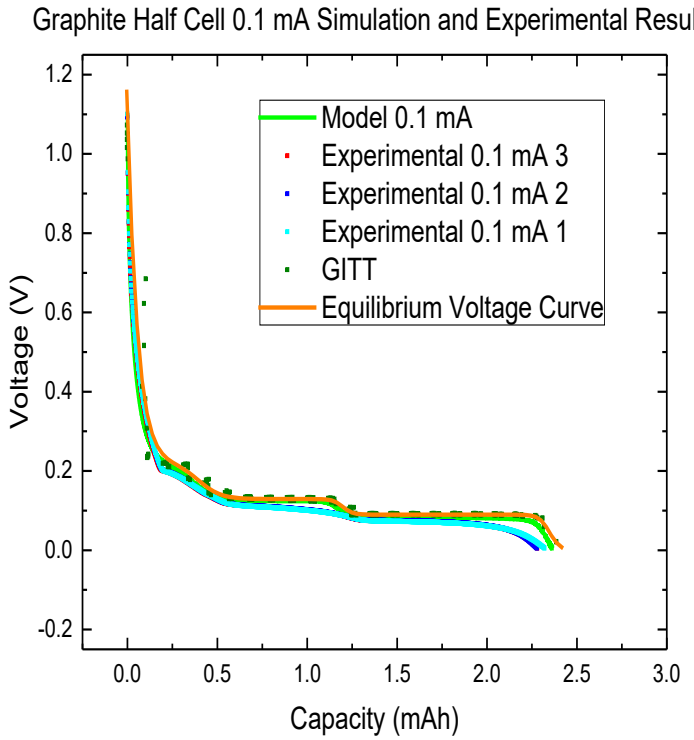

Figure 21 Graphite vs. lithium coin cell simulation and experimental discharges at 0.1 mA compared with the GITT data and the graphite equilibrium voltage curve equation used in the model.

The simulation results closely follow the equilibrium voltage curve put into the model. While the experimental results do show some differences from the simulation results, the simulation results using the parameter estimates obtained in this thesis are within 40 mV of the experimental discharge data at 0.1 mA.

To gain a better understanding of how these physical parameter estimates compare to experimental data, simulation results were compared to experimental data at higher C-rates. Figure 22 shows the experimental data for a 0.2 mA discharge compared with the simulation results.

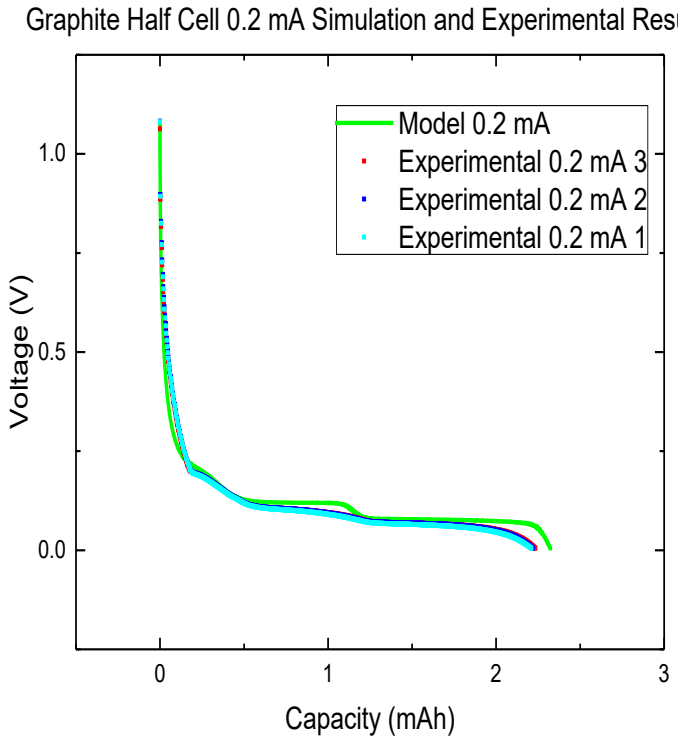

Figure 22 0.2 mA discharge comparison of simulation results and experimental data.

The simulation results and experimental data at 0.2 mA are still in good agreement. The capacity of the simulation results at 0.2 mA is 2.32 mAh compared to 2.22 mAh on average for the experimental data. The capacity values at 0.2 mA decreased by approximately the same amount from the capacity values at 0.1 mA. The capacity at 0.1 mA for the simulation results was 2.37 mAh and was 2.28 mAh on average for the experimental results. Though the difference between the voltage plateaus in the simulation and the experimental data is more pronounced at 0.2 mA than it was at 0.1 mA. Additionally, the voltage drop between 1 V and 0.25 V in the simulation is steeper than in the experimental data and the difference is more pronounced at 0.2 mA than it was at 0.1 mA. However, this comparison still shows

that the estimated physical parameter set is a good starting place for further refinement through fitting to experimental data.

Figure 23 shows the experimental data and the simulation results for discharge at 0.4 mA.

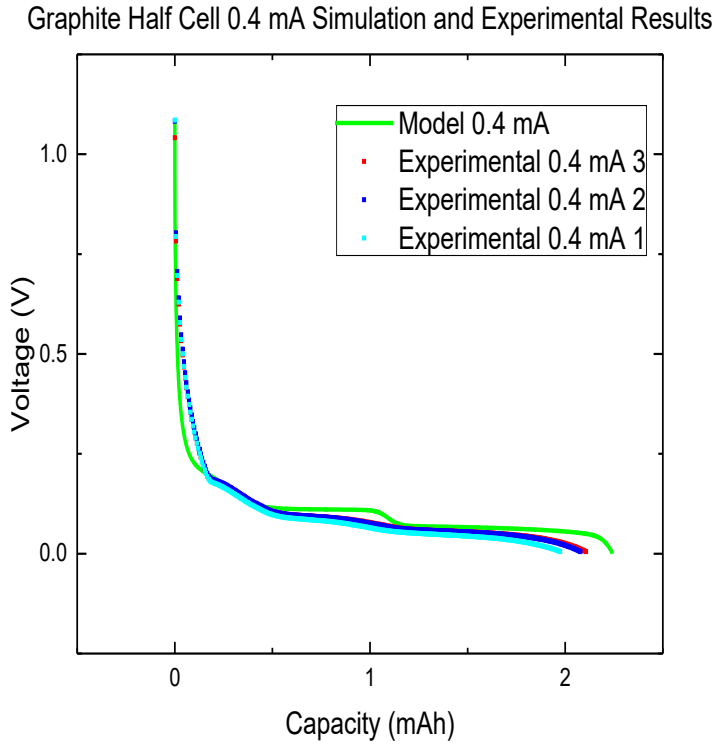

Figure 23 Experimental data and simulation results for 0.4 mA discharge.

The simulation results and experimental data continue to show the same trends as those seen at 0.2 mA and 0.1 mA. The difference in the voltage drop between 1 V and 0.25 V again is steeper in the simulation results than in the experimental data. Additionally, the difference between the voltage plateaus in the simulation and the experimental data is more pronounced as the C-rate increases. The capacity for the simulation results at 0.4 mA was

2.24 mAh and 2.05 mAh on average for the experimental data. While the differences in the simulation results capacities and the experimental data capacities at 0.1 mA and 0.2 mA was fairly similar, the difference in the simulation results capacities, 0.08 mAh, is less than the difference in the experimental data capacities, 0.17 mAh, between the 0.2 mA discharge and the 0.4 mA discharge. Part of this is due to the variance in the experimental data capacities between cells. The cell 1 capacity decreased more from 0.2 mA to 0.4 mA than the capacities of cells 2 and 3. This could be because of a larger ohmic resistance, perhaps due to increased contact resistance. One of the challenges of using coin cells is manufacturing reproducible cells. Commercial cells are more consistent in their results due to the precision with which they are manufactured. This is one example of how commercial cells are preferable to coin cells for comparing experimental data to simulation results.

Figure 24 shows the experimental data and the simulation results for the 0.67 mA and 1 mA discharges.

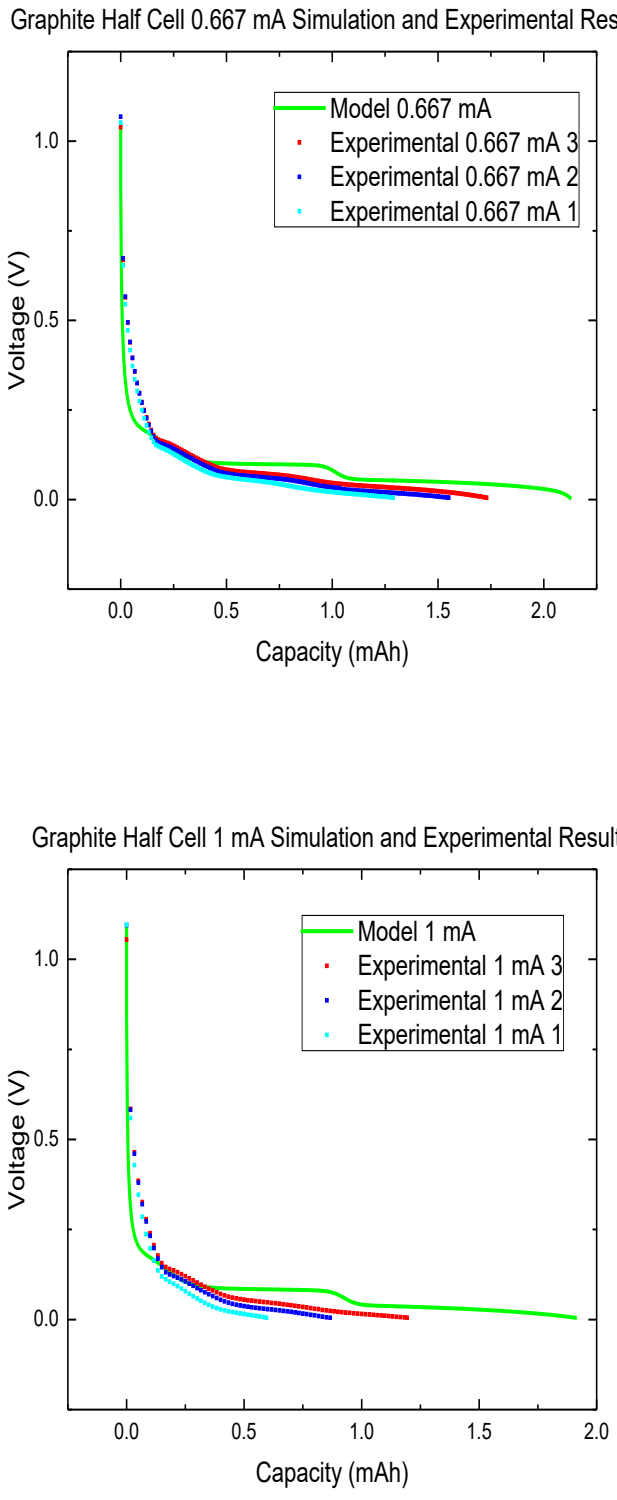

Figure 24 Experimental data and simulation results for 0.67 mA discharge (top) and 1 mA discharge (bottom).

At higher discharge rates the experimental discharge capacity decreases more than the simulation discharge capacity. The capacities for each of the experimental cells and the simulation results with increasing discharge rate is shown in Table 3.

Table 3 Capacity vs. Rate of Discharge

Discharge Current (mA)	Cell 2 Discharge Capacity (mAh)	Cell 3 Discharge Capacity (mAh)	Cell 4 Discharge Capacity (mAh)	Average Cell Discharge Capacity (mAh)	Simulation Discharge Capacity (mAh)
0.1	2.32	2.28	2.28	2.29	2.36
0.2	2.21	2.22	2.23	2.22	2.32
0.4	1.97	2.08	2.11	2.05	2.24
0.667	1.29	1.55	1.73	1.52	2.12
1	0.60	0.87	1.19	0.89	1.91

The experimental discharge capacity decreases at a higher rate as the discharge rate increases than the simulation discharge capacity. The difference between the experimental discharge capacity at for the 0.1 mA discharge and for the 1 mA discharge is 1.4 mAh while the same difference for the simulation discharge capacity is only 0.45 mAh. The estimated physical parameters do not capture the experimental discharge capacity decrease with increasing discharge rate. However, the estimated physical parameter set does provide a starting place for further refinement of the parameter set by fitting simulation results to experimental data.

In this chapter, the simulation results using the parameter estimates obtained in this thesis are compared to experimental data. While there are areas where the simulation results do not match the experimental data, the comparison of the simulation results with the experimental data does show that the parameter estimates are a good starting place for

further refinement. The parameter estimates provide a starting place for refining parameters by fitting experimental data that will increase the probability of finding an accurate finalized parameter set.

CHAPTER 6. CONCLUSIONS AND FUTURE WORK

Batteries and other electrochemical systems are becoming wide-spread as power sources in many industries. Consumer demands require that electrochemical systems continue to improve to become viable in new industries and to continue to improve in well-established industries. Electrochemical research includes the modeling of electrochemical systems to both predict performance and to improve the understanding of the physics. Understanding the physics of electrochemical systems can help with identifying limitations and areas of improvement. However, physics-based models are required for gaining insight into the physical characteristics of the electrochemical system. Physics-based models' parameters are found by fitting the model to experimental data. While a physics-based model that fits experimental data well is a good indicator that the parameters are accurate, there is a risk that the parameters identified through fitting are inaccurate or even infeasible because of the complexity of the model. The physical insight gained into an electrochemical system is only as valuable as the accuracy of the physical parameters identified for the model. Parameter identification for physics-based models should prioritize finding the most accurate parameter set possible, rather than focusing only on fitting the experimental data.

A process for parameter identification has been demonstrated in this thesis that will lead to a higher probability of obtaining an accurate finalized parameter set. Ideally, all parameters would be physically measured, but while this is possible for parameters like electrode thickness, there are many parameters that cannot be physically measured. These parameters are determined by fitting the model to experimental data. In the past, parameter

estimates used as the initial input for the fitting process were often obtained from the literature. However, the reliability of the literature to provide good estimates for parameters is questionable due to the amount of variance that exist. At times a parameter in the literature can vary by orders of magnitude. Even for well-established materials like $LiMn_2O_4$ or graphite. Also under consideration is the modeling of new materials for which estimates for parameters cannot be obtained from the literature. A process to obtain reasonable estimates for each of the parameters in a physics-based model would increase the chances of obtaining an accurate parameter set by fitting the model to experimental data.

This thesis has outlined a process for obtaining estimates for parameters in a physics-based model. The process begins by identifying the electrochemical system being modeled, the physics-based model being used, and then identifying all of the parameters necessary for the model. After the parameters have been identified, the parameters that can be measured with the experimental capabilities of the modeler should be measured. Another characterization step is to calculate the theoretical capacity of the electrochemical system. This allows the modeler to calculate what current to use for the formation cycles of the electrochemical system. The modeler must also establish what voltage limits will be used for the electrochemical system. Once the system has been through the formation cycles, the modeler can perform the Galvanostatic Intermittent Titration Technique (GITT) to estimate the equilibrium voltage of the electrochemical system over the voltage limits previously identified. The modeler decides how many steps should be taken at what C-rate and how long of a rest time is needed for the electrochemical system to reach equilibrium.

Once they have gathered the planned number of points, those points can be fit to an equation for inputting the equilibrium voltage curve into the model.

While the GITT is being performed, electrochemical impedance spectroscopy (EIS) can be performed on the electrochemical system after each step of the GITT. This EIS data can be fit to an equivalent circuit designed by the modeler to estimate other parameters of the electrochemical system. After obtaining estimates for as many parameters as possible, estimates for the remaining parameters can be obtained from the literature trying to find values for materials that are as close as possible to the materials being used in the electrochemical system.

After estimates have been obtained for all of the parameters necessary for the physics-based model, the model can be compared to experimental data to see how the estimated parameter set compares to experimental data. At that point, the parameters should be adjusted to final values by fitting the simulation output to the experimental data. The process for fitting the experimental data should also be further defined to prioritize finding an accurate parameter set, however that process is not defined in this thesis. Once the modeler has obtained a finalized parameter set by fitting the experimental data selected, the model should be validated using a validation set of data to ensure that the model fits data other than the original data used for parameter fitting. Once the model has been validated, the physics-based model can be extrapolated to other experimental conditions and be used to elucidate the physics of the electrochemical system with more confidence.

This thesis demonstrated the estimation process for a graphite vs. lithium coin cell. The necessary physical parameters for this electrochemical system to be modelled by a Doyle-

Fuller Newman model were identified in Chapter 2. In Chapter 3, an SEM image was taken of the graphite electrode to obtain the geometric parameters for the electrochemical system. The GITT process used to identify the equilibrium voltage curve of the graphite electrode vs. state of charge (SOC) was also explained. Chapter 4 explained the procedure for collecting EIS data along with the equivalent circuit used for fitting the EIS data. The equivalent circuit elements were related to the electrolyte conductivity, the exchange current densities of the lithium foil and the graphite electrode, and the solid phase diffusivity of lithium in the graphite electrode through equations used to estimate physical parameters from equivalent circuit parameters found in the literature. Chapter 5 compiled all of the parameter estimates obtained in this thesis and used them as input to a DFN model coded in gPROMs. The model output was compared to experimental discharges of the lithium vs. graphite coin cells at various C-rates. The comparison showed that for low C-rates the experimental and simulation data matched well. However, at moderate C-rates the amount of capacity for the experimental cells was much less than the capacity of the simulation cells. This indicates that some of the parameter estimates obtained need further refinement to better fit discharge data at moderate C-rates or that the model is lacking some of the physics present in the coin cell. However, the parameter estimates obtained in this thesis proved to be a reasonable starting place for parameter identification and provide a greater chance of finding an accurate final parameter set due to the manner in which the estimates were obtained.

This thesis has outlined a process for obtaining estimates for a physics-based model for an electrochemical system using SEM, GITT, and EIS data. The ability to obtain estimates for each of the parameters of an electrochemical system improves the probability of finding

an accurate parameter set, and reduces the possibility of finding infeasible parameter sets. The estimates that are obtained give the modeler additional information to be able to constrain the parameter fitting and to help the fitting program by giving better initial guesses. Being able to obtain estimates independently rather than from the literature helps to improve confidence in the estimates obtained and to be able to obtain estimates for new materials not available in the literature.

Future work remains to compare the model using parameter estimates as inputs to a wider variety of experimental data. The process could also be used to estimate parameters for a commercial cell rather than a coin cell as coin cells have issues of reproducibility and, because of significant internal losses, do not perform well in high C-rate experiments. Once parameter estimates have been established for a system, a more detailed process for fitting a model to experimental data could similarly be outlined to improve the chances of obtaining the most accurate final parameter set. For example, the process could specify which parameters to refine by fitting what sets of experimental data. Also deciding what experimental data to use for fitting and what experimental data to use for validating the physics-based model. While this thesis outlines the process for obtaining parameter estimates, the steps in between parameter estimates and the final parameter set needs to be further detailed and outlined to improve the accuracy of the final parameter set obtained.

REFERENCES

[1] Mobile Fact Sheet https://www.pewresearch.org/internet/fact-sheet/mobile/ (accessed Dec 11, 2019).

[2] Vimmerstedt, L., Brown, A., Newes, E., Markel, T., Schroeder, A., Zhang, Y., … Johnson, S. (2015). Transformative Reduction of Transportation Greenhouse Gas Emissions. Opportunities for Change in Technologies and Systems. *NREL*. doi: 10.2172/1215028

[3] Gebrehiwot, M., & Van den Bossche, A. (2015). Driving Electric Vehicles: as Green as the Grid. [Proceedings Paper]. *Proceedings of the 2015 12th Ieee Africon International Conference - Green Innovation For African Renaissance (Africon)*.

[4] Mamen, A., & Supatti, U. (2017). A Survey of Hybrid Energy Storage Systems Applied for Intermittent Renewable Energy Systems. [Proceedings Paper]. *2017 14th International Conference on Electrical Engineering/electronics, Computer, Telecommunications and Information Technology (Ecti-Con)*, 729-732.

[5] Saritha, D. (2019). A concise review on the advancement of anode materials for Li-ion batteries. [Proceedings Paper]. *Materials Today-Proceedings, 19*, 726-730.

[6] Zhang, H., Armand, M., & Rojo, T. (2019). Review-Innovative Polymeric Materials for Better Rechargeable Batteries: Strategies from CIC Energigune. [Article|Proceedings Paper]. *Journal of the Electrochemical Society, 166*(4), A679-A686.

[7] Grazioli, D., Magri, M., & Salvadori, A. (2016). Computational modeling of Li-ion batteries. [Review]. *Computational Mechanics, 58*(6), 889-909.

[8] Plett, G. (2015). Battery Management Systems, Vol I: Battery Modeling. [Book]. *Battery Management Systems, Vol I: Battery Modeling*, 1-327.

[9] Chaturvedi, N., Klein, R., Christensen, J., Ahmed, J., & Kojic, A. (2010). Algorithms for Advanced Battery-Management Systems MODELING, ESTIMATION, AND CONTROL CHALLENGES FOR LITHIUM-ION BATTERIES. [Article]. *Ieee Control Systems Magazine, 30*(3), 49-68.

[10] Liebig, G., Gupta, G., Kirstein, U., Schuldt, F., & Agert, C. (2019). Parameterization and Validation of an Electrochemical Thermal Model of a Lithium-Ion Battery. [Article]. *Batteries-Basel, 5*(3).

[11] Safari, M., & Delacourt, C. (2011). Modeling of a Commercial Graphite/LiFePO4 Cell. [Article]. *Journal of the Electrochemical Society, 158*(5), A562-A571.

[12] Brady, N. W.; Gould, C. A.; West, A. C. Quantitative Parameter Estimation, Model Selection, and Variable Selection in Battery Science. *J. Electrochem. Soc.* **2020**, *167*, 013501.

[13] Yeduvaka, G., Spotnitz, R., & Gering, K. (2009). Macro-homogenous modeling of commercial, primary Li/MnO_2 Coin Cells [Article]. *ECS Transactions, 19*(16), 1-10.

[14] Santhanagopalan, S., Guo, Q., & White, R. (2007). Parameter estimation and model discrimination for a lithium-ion cell. [Article]. *Journal of the Electrochemical Society, 154*(3), A198-A206.

[15] Forman, J., Moura, S., Stein, J., & Fathy, H. (2012). Genetic identification and fisher identifiability analysis of the Doyle-Fuller-Newman model from experimental cycling of a LiFePO4 cell. [Article]. *Journal of Power Sources, 210*, 263-275.

[16] Smith, K., & Wang, C. (2006). Solid-state diffusion limitations on pulse operation of a lithium ion cell for hybrid electric vehicles. [Article]. *Journal of Power Sources, 161*(1), 628-639.

[17] Fang, W., Kwon, O., & Wang, C. (2010). Electrochemical-thermal modeling of automotive Li-ion batteries and experimental validation using a three-electrode cell. [Article]. *International Journal of Energy Research, 34*(2), 107-115.

[18] Schmalstieg, J., & Sauer, D. (2018). Full Cell Parameterization of a High-Power Lithium-Ion Battery for a Physico-Chemical Model: Part II. Thermal Parameters and Validation. [Article]. *Journal of the Electrochemical Society, 165*(16), A3811-A3819.

[19] Less, G., Seo, J., Han, S., Sastry, A., Zausch, J., Latz, A., et al. (2012). Micro-Scale Modeling of Li-Ion Batteries: Parameterization and Validation. [Article]. *Journal of the Electrochemical Society, 159*(6), A697-A704.

[20] Schmalstieg, J., Rahe, C., Ecker, M., & Sauer, D. (2018). Full Cell Parameterization of a High-Power Lithium-Ion Battery for a Physico-Chemical Model: Part I. Physical and Electrochemical Parameters. [Article]. *Journal of the Electrochemical Society, 165*(16), A3799-A3810.

[21] Ecker, M., Kabitz, S., Laresgoiti, I., & Sauer, D. (2015). Parameterization of a Physico-Chemical Model of a Lithium-Ion Battery II. Model Validation. [Article]. *Journal of the Electrochemical Society, 162*(9), A1849-A1857.

[22] Ecker, M.; Tran, T.K.D.; Dechent, P.; Kabitz, S.; Warnecke, A.; Sauer, D.U. Parameterization of a Physico-Chemical Model of a Lithium-Ion Battery I. Determination of Parameters. *J. Electrochem. Soc.* **2015,** *162*, A1836-A1848.

[23] Chu, Z., Jobman, R., Rodriguez, A., Plett, G., Trimboli, M., Feng, X., & Ouyang, M. (2020). A control oriented electrochemical model for lithium-ion battery. Part II: Parameter identification based on reference electrode. [Article]. *Journal of Energy Storage*, 27, 101101.

[24] gPROMS https://www.psenterprise.com/products/gproms (accessed Jan 22, 2020)

[25] Liaw, B., Nagasubramanian, G., Jungst, R., & Doughty, D. (2004). Modeling of lithium ion cells - A simple equivalent-circuit model approach. [Article|Proceedings Paper]. *Solid State Ionics, 175*(1-4), 835-839.

[26] Haran, B., Popov, B., & White, R. (1998). Determination of the hydrogen diffusion coefficient in metal hydrides by impedance spectroscopy. [Article]. *Journal of Power Sources, 75*(1), 56-63.

[27] Schmidt, A., Bitzer, M., Imre, A., & Guzzella, L. (2010). Experiment-driven electrochemical modeling and systematic parameterization for a lithium-ion battery cell. [Article]. *Journal of Power Sources, 195*(15), 5071-5080.

[28] Wu, S., Zhang, W., Song, X., Shukla, A., Liu, G., Battaglia, V., et al. (2012). High Rate Capability of Li(Ni1/3Mn1/3Co1/3)O-2 Electrode for Li-Ion Batteries. [Article]. *Journal of the Electrochemical Society, 159*(4), A438-A444.

[29] Web of Science https://apps.webofknowledge.com/InboundService.do?customersID=RRC&mode=FullRecord&IsProductCode=Yes&product=WOS&Init=Yes&Func=Frame&DestFail=http%3A%2F%2Fwww.webofknowledge.com&action=retrieve&SrcApp=RRC&S

rcAuth=RRC&SID=8EVFh155x5yEZliHaF9&UT=WOS%3AA1993LG41000011 (accessed Dec 11, 2019).

[30] Doyle, M.; Fuller, T.F.; Newman, J. Modeling of Galvanostatic Charge and Discharge of the Lithium/Polymer/Insertion Cell. *J. Electrochem. Soc.* **1993**, *140*, 1526-1533.

[31] Doyle, M.; Fuller, T.F.; Newman, J. Simulation and Optimization of the Dual Lithium Ion Insertion Cell. *J. Electrochem. Soc.* **1994**, *141*, 1-10.

[32] Newman, J. S. (2004). *Electrochemical systems* (3rd ed.. ed.). Hoboken, N.J.: Hoboken, N.J. : J. Wiley. [33] Smart, M., & Ratnakumar, B. (2011). Effects of Electrolyte Composition on Lithium Plating in Lithium-Ion Cells. [Article]. *Journal of the Electrochemical Society, 158*(4), A379-A389.

[34] Kumaresan, K., Guo, Q., Ramadass, P., & White, R. (2006). Cycle life performance of lithium-ion pouch cells. [Article]. *Journal of Power Sources, 158*(1), 679-688.

[35] WEPPNER, W., & HUGGINS, R. (1977). DETERMINATION OF KINETIC-PARAMETERS OF MIXED-CONDUCTING ELECTRODES AND APPLICATION TO SYSTEM LI3SB. [Article]. *Journal of the Electrochemical Society, 124*(10), 1569-1578.

[36] Rashid, M., Pathan, T., McGordon, A., Kendrick, E., & Widanage, W. (2019). Investigation of hysteresis and relaxation behaviour in graphite and LiNi0.33Mn0.33Co0.33O2 electrodes. [Article]. *Journal of Power Sources, 440*.

[37] Ender, M. (2015). An extended homogenized porous electrode model for lithium-ion cell electrodes. [Article]. *Journal of Power Sources, 282*, 572-580.

[38] Fuller, T.F.; Harb, J.N. Electrochemical Engineering. Wiley 2018.

[39] Hess, M., Lebraud, E., & Levasseur, A. (1997). Graphite multilayer thin films: a new anode material for Li-ion microbatteries synthesis and characterization. [Article|Proceedings Paper]. *Journal of Power Sources, 68*(2), 204-207.

[40] Park, M., Zhang, X., Chung, M., Less, G., & Sastry, A. (2010). A review of conduction phenomena in Li-ion batteries. [Review]. *Journal of Power Sources, 195*(24), 7904-7929.

[41] Lundgren, H., Behm, M., & Lindbergh, G. (2015). Electrochemical Characterization and Temperature Dependency of Mass-Transport Properties of LiPF6 in EC:DEC. [Article]. *Journal of the Electrochemical Society, 162*(3), A413-A420.

[42] Lee, S., Jung, U., Kim, Y., Kim, M., Ahn, D., & Chun, H. (2002). A study of electrochemical kinetics of lithium ion in organic electrolytes. [Article]. *Korean Journal of Chemical Engineering, 19*(4), 638-644.

[43] Mendoza-Hernandez, O., Ishikawa, H., Nishikawa, Y., Maruyama, Y., Sone, Y., & Umeda, M. (2014). State of Charge Dependency of Graphitized-Carbon-Based Reactions in a Lithium-ion Secondary Cell Studied by Electrochemical Impedance Spectroscopy. [Article|Proceedings Paper]. *Electrochimica Acta, 131*, 168-173.

[44] Jow, T., Marx, M., & Allen, J. (2012). Distinguishing Li+ Charge Transfer Kinetics at NCA/Electrolyte and Graphite/Electrolyte Interfaces, and NCA/Electrolyte and LFP/Electrolyte Interfaces in Li-Ion Cells. [Article]. *Journal of the Electrochemical Society, 159*(5), A604-A612.

[45] BOTTELBERGHS, P., & BROERS, G. (1976). INTERFACIAL IMPEDANCE BEHAVIOR OF POLISHED AND PAINT PLATINUM-ELECTRODES AT NA-2WO-4-NA-2M0O-4 SOLID ELECTROLYTES. [Article]. *Journal of Electroanalytical Chemistry, 67*(2), 155-167.

[46] impedance.py https://impedancepy.readthedocs.io/en/latest/ (accessed Mar 19, 2020)

[47] PyCharm https://www.jetbrains.com/pycharm/ (accessed Mar 19, 2020)

[48] Tapesh, J. Capacity and Power Fade in Lithium-Ion Batteries. Ph.D. Dissertation. Georgia Institute of Technology **2016**.

[49] Garche Jürgen. (2009). *Encyclopedia of electrochemical power sources*. Amsterdam: Elsevier.

[50] Bruggeman, D. (1935). Calculation of various physics constants in heterogenous substances I Dielectricity constants and conductivity of mixed bodies from isotropic substances. [Article]. *Annalen Der Physik, 24*(7), 636-664.

[51] Doyle, M., & Fuentes, Y. (2003). Computer simulations of a lithium-ion polymer battery and implications for higher capacity next-generation battery designs. [Article]. *Journal of the Electrochemical Society, 150*(6), A706-A713.

[52] Star, A., & Fuller, T. (2019). Combining tomographic imaging and in silico computation for rapid effective PEMFC cathode transport characterization. [Article]. *Chemical Engineering Science, 201*, 309-318.

[53] Doyle, M., Meyers, J., & Newman, J. (2000). Computer simulations of the impedance response of lithium rechargeable batteries. [Article]. *Journal of the Electrochemical Society, 147*(1), 99-110.

[54] Yu, P.; Popov, B.N.; Ritter, J.A.; White, R.E. Determination of the Lithium Ion Diffusion Coefficient in Graphite. *J. Electrochem. Soc.* **1999,** *146,* 8-14.

[55] Levi, M., & Aurbach, D. (1997). Diffusion coefficients of lithium ions during intercalation into graphite derived from the simultaneous measurements and modeling of electrochemical impedance and potentiostatic intermittent titration characteristics of thin graphite electrodes. [Article]. *Journal of Physical Chemistry B, 101*(23), 4641-4647.

[56] Funabiki, A., Inaba, M., Ogumi, Z., Yuasa, S., Otsuji, J., & Tasaka, A. (1998). Impedance study on the electrochemical lithium intercalation into natural graphite powder. [Article]. *Journal of the Electrochemical Society, 145*(1), 172-178.